Theoretical Investigation of Thermal Decomposition of Peroxidized Coelenterazines with and without External Perturbations†

Hiroshi Isobe,* Syusuke Yamanaka, Mitsutaka Okumura, and Kizashi Yamaguchi

Department of Chemistry, Graduate School of Science, Osaka University, Toyonaka, Osaka 560-0043, Japan

Received: June 9, 2009; Revised Manuscript Received: October 3, 2009

Thermal decomposition of peroxidized coelenterazines with and without external perturbations has been studied theoretically using the hybrid density functional theory (B3LYP) and the Coulomb-attenuating method (CAM). Possible roles of a hydrogen-bonding interface constituted by amino acid residues in the coelenterazine-biding site of aequorin are addressed by using simple model clusters with a polarizable continuum model to grasp some important aspects that may affect the electronic mechanism operating within the photoprotein. Calculations have revealed that the electronic property and stability of the peroxide are greatly affected by its protonation state and/or environmental effects, such as a polarizing medium and specific (localized) short-range electrostatic interactions, which may be critical for the bioluminescence activity. Theory highlights two mechanisms by which the neutral species can be activated, which otherwise decomposes by a homolytic O−O dissociation with a high barrier. In the first mechanism, the Tyr82-His16-Trp86 triad motif facilitates the deprotonation process of the phenolic OH group at the C_6 position of the coelenterazine and thereby makes it a sufficiently good electron donor to activate the O−O bond. In the second mechanism, intramolecular charge transfer is accomplished within the neutral peroxide by a proton delivery mediated via another triad motif, Tyr184-His169-Trp173, without the activation of the substrate itself. The combination of the first and second mechanisms leads to complete electron transfer for the formation of a radical pair as a local intermediate stabilized by the nearby triad motifs.

1. Introduction

Many calcium-activated photoproteins appear in nature, such as aequorin,[1] obelin,[2] thalassicolin,[3] mitrocomin,[4] clytin,[5] mnemiopsin, and berovin.[6] Among these, aequorin is first isolated from marine bioluminescent organisms, the jellyfish *Aequoria*,[1a] and since then, enormous effort has been devoted to its unique property to emit visible light in the presence of a trace amount of Ca^{2+} ions but without molecular oxygen or any other cofactor.[1] As a result, the aequorin has been recognized as a useful indicator for studying intracellular Ca^{2+} ions.[7]

The aequorin consists of an apoprotein, which is 189 amino acid residues in length and contains four helix−loop−helix "EF-hand" domains,[8] a noncovalently bound coelenterate-type luciferin coelenterazine, **1H**, and a molecular oxygen (O_2). A recent X-ray crystallographic study revealed that **1H** and O_2 are both incorporated into the apoprotein to form a coelenterazine−2-hydroperoxide adduct, **2**, which is stabilized by a hydrogen-bonding array with Tyr184 and His169, as shown in Figure 1.[9] Scheme 1 shows the commonly accepted molecular mechanism by which bioluminescence occurs. In the absence of additional O_2, the binding of Ca^{2+} ions to the two of the four EF-hand structures of aequorin triggers a series of events that completes the oxidative decarboxylation of **1H**, yielding an emission of blue light ($\lambda_{max} \approx 465$ nm), a carbon dioxide (CO_2), and blue fluorescent protein (BFP), which contains coelenteramide, **4**, noncovalently bound to apoprotein.[10,11] The interpretations are consistent with the well-characterized chemistries of synthetic coelenterazine analogues.[12] A consensus has been reached that four-membered α-peroxylactone, **3**, known also as dioxetanone, is a key structure to generate an electronically excited state of **4**. The catalysis by the protein environment guarantees the efficient conversion of chemical energy released in the oxidation of the substrate into photon energy (bioluminescence quantum yield is 0.2),[11] which is, otherwise, very difficult to achieve (chemiluminescence quantum yield is only 0.002 in DMSO).[13]

Knowledge of the roles of key amino acid residues is important to understand the bioluminescence mechanism. The effects of the site-directed mutagenesis of conserved histidine, cysteine, proline, and tryptophan residues in apoprotein on bioluminescence activity were examined and discussed in terms of their functional roles in aequorin.[14] Cysteine residues were found to play an important role in the regeneration of aequorin but not in its catalytic activity.[14a] A C-terminal proline was required for bioluminescence activity of the photoprotein.[14b] Five specific amino acid residues, His16, His58, His169, Trp108, and Trp173 in apoprotein were observed to have a profound effect on the bioluminescence activity.[14d,f] Among these, the modifications of His169 led to complete loss of activity.[14d] The mutation of Trp86 to phenylalanine displayed a bimodal emission with a second band maximum at 400 nm.[14f] Semisynthetic aequorins that are composed of the native apoaequorin and coelenterazine analogues were also utilized to investigate the important structural features of the side groups at the C_2, C_6, and C_8 positions of the imidazopyrazinone ring.[15,16] The structure−activity relationships were interpreted in terms of specific interactions between the peroxidized coelenterazine and the surrounding protein environment.[1d,15] The importance of the stereochem-

† Part of the "Vincenzo Aquilanti Festschrift".

* To whom correspondence should be addressed. E-mail: isobe@chem.sci.osaka-u.ac.jp.

10.1021/jp905401b
Published on Web 10/30/2009

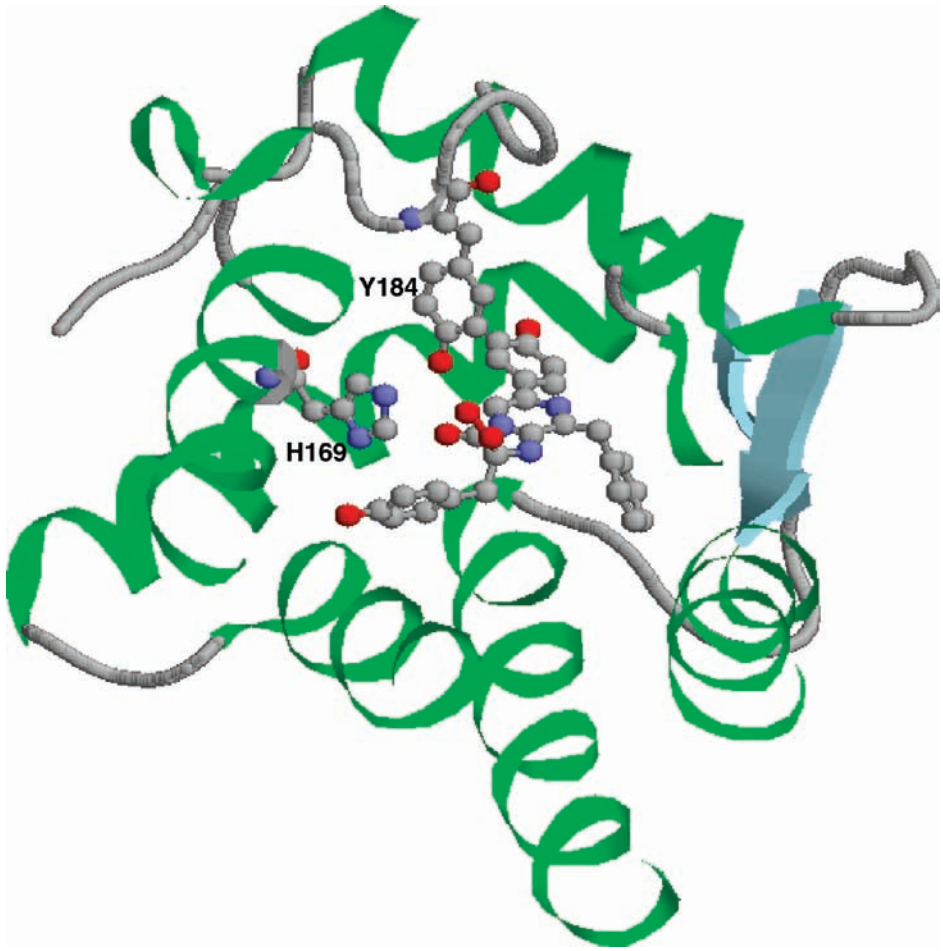

Figure 1. Coelenterazine-binding site of aequorin, as determined by the X-ray crystallographic study (PDB code 1EJ3).[9]

SCHEME 1

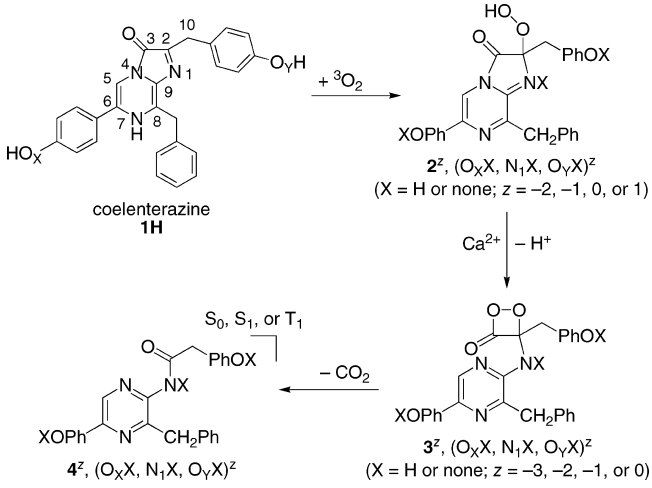

istry of the 4-hydroxyphenyl group at the C_6 position and hydrophobic interactions at the C_2 and C_8 positions were suggested and later confirmed by the X-ray crystal structure.[9] In the past, there have been debates about the nature of the light emitter involved in bioluminescence.[12d,17] The fluorescence properties of **4** and its analogues have been extensively studied in various organic solvents, and five kinds of emitters have so far been proposed,[17b] which include neutral, phenoxide anion (or ion pair), amido anion, and so on.

In this study, we have explored some important events in Scheme 1 to understand detailed electronic mechanisms by quantum chemical calculations, which can provide information about electronic properties and energetics of unstable intermediates and transition states and thereby may serve as an essential and complementary insight to experiment. This study is devoted first to the thermal decomposition of isolated peroxidized coelenterazines $\mathbf{3}^z$ (z is the total charge) with various protonation states, (O_XX, N_1X, O_YX)^z (X = H or none), with the aim of understanding the influence of the protonation state on the electronic properties and chemical behaviors of the labile peroxides without any perturbations. Next, the possible roles of hydrogen bonding by amino acid residues are addressed by using simple model complexes to grasp some important aspects that may affect the electronic mechanism operating within the coelenterazine-binding site of aequorin. We will show that environmental effects significantly affect the electronic characteristics of the dissociating peroxide. Finally, limitations of the present model are posed and some modifications are suggested to accommodate experimental facts.

2. Computational Details and Theoretical Backgrounds

This study is divided in two parts. In the first part, the thermolysis of peroxidized coelenterazines $\mathbf{3}^z$ (cyclic dioxetanone or open-chain 3-peroxide intermediates) as isolated molecules is investigated by full geometry optimizations without any constraints. Possible protonation states, as shown in Figure 2, were considered to clarify their influence on the electronic properties and stabilities of the peroxides. The effects of the protonation at the N_7 position of $\mathbf{3}^z$ were not

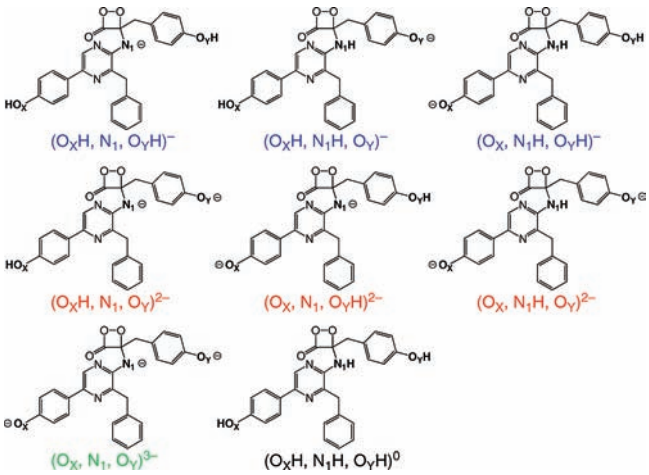

Figure 2. Protonation states of peroxidized coelenterazines $\mathbf{3}^z$ ($z = -3, -2, -1, 0$) considered by us.

investigated in this study; the results may be reported elsewhere. There are vast numbers of conformational isomers of $\mathbf{3}^z$ associated with the orientations of three side groups, (4-hydroxyphenyl)methyl, 4-hydroxyphenyl, and benzyl groups that are attached to the C_2, C_6, and C_8 positions of the imidazopyrazinone ring and/or the rotation about the N_1-C_2 and C_2-C_{10} bonds, and so on. To maintain as closely as possible the same conformation as the one found at the recently determined X-ray crystallographic structure (Protein Data Bank, accession code 1EJ3),[9] geometry optimizations were done by directly adding H atoms and an O_2 molecule to the coelenterazine skeleton taken from the X-ray structure and then allowing its geometry to relax. The second part is devoted to the investigation of the effects of hydrogen bonds by three amino acid residues located in the vicinity of the oxido anion moiety of peroxidezed coelenterazines, $\mathbf{3}^-$, and its regioisomer. Constraint geometry optimizations of these model clusters were performed with some atoms fixed to their X-ray positions to avoid a large disorder that would be impossible in the actual biological system.

For isolated molecules (which will be discussed in the first part), all geometry optimizations were performed with the Gaussian 03[18] by using the unrestricted (U) B3LYP (UB3LYP) method[19] with the 6-31+G(d) basis set.[20] Frequency calculations were performed to verify the nature of all stationary points and to derive zero-point vibrational corrections (ZPC) and thermodynamics effects at 298 K by statistical mechanics calculations. For model complex systems (which will be discussed in the second part), geometry optimizations were performed with UB3LYP/6-31G(d), and the final energetics was further corrected by single-point calculations with the CPCM-UAKS model implemented in the Gaussian 03.[21] A dielectric constant (ε) of 4.0 was used to simulate a hydrophobic environment of a protein interior.[22] Additionally, we applied the long-range corrected Coulomb-attenuating method (CAM)[23] to the exploration of a radical pair generated by complete electron transfer, since the B3LYP functional does not describe a correct asymptotic behavior of the exchange potential.[24] CAM-B3LYP (VWN5) calculations were performed with a modified version of the GAMESS program package.[25]

To make a theoretical interpretation of the electronic characteristics of transition structures, symmetry-adapted natural orbitals (ϕ_i) were determined by diagonalizing the spin-traced first-order density matrices [$\rho(\mathbf{r}',\mathbf{r})$] of broken-symmetry solutions ($\psi^{\pm}$, corresponding orbitals),[26] as shown in eq 1, in which n_i is the occupation number of ϕ_i

$$\rho(\mathbf{r}',\mathbf{r}) = \sum_i [\psi_i^+(\mathbf{r}')\,\psi_i^{+*}(\mathbf{r}) + \psi_i^-(\mathbf{r}')\,\psi_i^{-*}(\mathbf{r})]$$
$$= \sum_i n_i \phi_i(\mathbf{r}')\,\phi_i^*(\mathbf{r}) \quad (1)$$

In a diradicaloid species, highest occupied (ϕ_{HONO}) and lowest unoccupied (ϕ_{LUNO}) natural orbitals appear in a pair with fractional occupation numbers,1 $\pm \langle\psi^+|\psi^-\rangle$. We used these paired orbitals to analyze the electronic characteristics for open-shell diradicaloid transition structures. The diradical character, y, can be measured by twice the weight of doubly excited configuration in the CI terminology, which is formally expressed by the occupation number of ϕ_{HONO} (n_{HONO}) in terms of the spin-projected UDFT wave function, Ψ_{PUDFT}, as shown in eqs 2a and 2b.[27]

$$\Psi_{PUDFT} = N[|\psi^+\bar{\psi}^-\rangle - |\bar{\psi}^+\psi^-\rangle]$$
$$= C_G|\phi_{HONO}\bar{\phi}_{HONO}\rangle - C_D|\phi_{LUNO}\bar{\phi}_{LUNO}\rangle \quad (2a)$$

$$y \equiv 2C_D^2$$
$$= (n_{HONO}^2 - 4n_{HONO} + 4)/(n_{HONO}^2 - 2n_{HONO} + 2) \quad (2b)$$

3. Results and Discussion

3.1. Influence of Protonation State on the Thermal Decomposition of Peroxidized Coelenterazine. We shall begin by considering the thermal decomposition of peroxidized coelenterazine, $\mathbf{3}^z$, as an unperturbed molecule, which is formed from the addition reaction of O_2 into the C_2 position of coelenterazine, **1H**. The chemical consequences of the reaction are directly affected by the charge and spin distributions of a dissociating peroxide, which themselves depend on the protonation state of the substrate and environment.[28] The relation between the protonation state and the electronic mechanism for the thermolysis of isolated dioxetanone $\mathbf{3}^z$ is the point that needs to be clarified in this subsection. Figure 2 shows the protonation states of $\mathbf{3}^z$ considered by us, which include one neutral, three monoanion, three dianion, and one trianion states, depending on whether three titratable sites (O_X, N_1, and O_Y positions) are protonated or not; henceforth, the protonation state is specified as $(O_XX, N_1X, O_YX)^z$, in which X = H if the position is protonated and z is the total charge ($z = -3, -2, -1$, or 0). Provided that there are many aromatic residues (three tryptophans and three tyrosines) and benzene rings (three side groups of $\mathbf{3}^z$), two of which have a stacked or T-shape conformation with a histidine residue, the neutral and monoanion states are the most likely candidates for the protonation-state identity of $\mathbf{3}^z$ in the actual photoprotein, since these protonation states might be stabilized through cation$-\pi$ interactions in a cationic hydrophobic pocket.[29,30] If the protein pocket is neutral, however, the dianion state cannot be entirely ruled out.[30] The trianion state is not likely to be involved in the bioluminescence, and therefore, is considered here only for completeness. Table 1 corrects computed activation barriers of decomposition including ZPC, peroxide O−O bond lengths ($r_{OO}^{\ddagger}$) and diradical characters ($y^{\ddagger}$) at transition structures (TS), along with the classification of decomposition mechanisms for all species considered. Figure 3 summarizes highest occupied and lowest unoccupied natural

TABLE 1: Computed Activation Energies, O−O Bond Lengths and Diradical Characters at Transition Structures, and the Classification of Decomposition Mechanisms for the Thermolysis of Isolated Dioxetanones 3[z], at the B3LYP/6-31+G(d) Level

protonation state	$\Delta E^{\ddagger}$ + ZPC[a]	$r_{OO}^{\ddagger}$ [b]	$y^{\ddagger}$ [c]	type[d]
$(O_XH, N_1H, O_YH)^0$	16.4	1.987	11.1	HD (FR)
$(O_XH, N_1, O_YH)^-$ higher-lying TS	24.6	1.935	5.7	HD (FR)
$(O_XH, N_1, O_YH)^-$ lower-lying TS	7.8	1.807	1.7	CT (AR)
$(O_XH, N_1H, O_Y)^-$	1.5	1.628	0.4	CT (AR)
$(O_X, N_1H, O_YH)^-$	1.5	1.647	0.2	CT (AR)
$(O_XH, N_1, O_Y)^{2-}$	7.2	1.771	1.4	CT (AR)
$(O_X, N_1, O_YH)^{2-}$	−5.5,[e] 6.4[f]	1.671	0.05	CT′(AR)
$(O_X, N_1H, O_Y)^{2-}$	4.2	1.695	0.6	CT (AR)
$(O_X, N_1, O_Y)^{3-}$	5.4	1.747	0.5	CT (AR)

[a] Activation energies including zero-point correction ($\Delta E^{\ddagger}$ + ZPC) are given in kcal mol^{-1}. [b] O−O bond lengths at TSs ($r_{OO}^{\ddagger}$) are given in angstroms. [c] Diradical characters at TSs ($y^{\ddagger}$) are given in %. [d] HD represents homolytic diradical mechanism, CT charge-transfer diradical mechanism, FR forbidden-radical mechanism, and AR allowed-radical mechanism. [e] Relative to cyclic dioxetanone intermediate, $\mathbf{3}^{2-}$ (see Figure 5). [f] Relative to open-chain 3-peroxide intermediate nascent from $\mathbf{3}^{2-}$ (see Figure 5).

orbitals, ϕ_{HONO} and ϕ_{LUNO}, and their occupation numbers, n_{HONO} and n_{LUNO}, at the TSs for the neutral, monoanion, and dianion states.

The neutral species, $(O_XH, N_1H, O_YH)^0$, in which all three titratable sites are protonated, has a relatively high activation barrier of decomposition (16.4 kcal mol^{-1}). At the equilibrium geometry of **3**, a bonding σ_{OO} orbital and an anitibonding σ_{OO}* orbital of the peroxide bond are formed by the interaction between two overlapping oxygen p orbitals that point along the bond axis. The former is stabilized and the latter is destabilized relative to the nonbonding level. As a result, only the former is occupied by a pair of up- and down-spin electrons. The elongation of the O−O bond, however, increases sharply the energy of the σ_{OO} orbital, while decreasing that of the σ_{OO}* orbital, as indicated by an orbital-symmetry-forbidden character for the [2 + 2] retrocycloaddition. This large increase in the energy of the filled orbital is the origin of the high barrier. At the same time, energetically unfavorable electrostatic repulsion caused by the confinement of two electrons into the σ_{OO} orbital is relieved by mixing the σ_{OO}* orbital with the σ_{OO} orbital, one in-phase and one out-of-phase, as shown in eq 3, in which ω is the orbital mixing angle.

$$\psi^{\pm} = \cos\omega\sigma_{00} \pm \sin\omega\sigma_{00}^{*} \quad (3)$$

ω is 0° for the closed-shell configuration, while ω ranges from 0° to 45° if the electron repulsion exceeds the effect of the σ_{OO}−σ_{OO}* orbitals splitting. The proper amount of the mixing of the orbitals makes the occupation numbers of HONO (σ_{OO}) and LUNO (σ_{OO}*) fractional, since $n = 1 \pm \cos 2\omega$, indicating a $\sigma_{OO}^2 \rightarrow \sigma_{OO}^{*2}$ pseudo double excitation, and thereby, it causes a decrease in ionic character in the wave function. Consequently, as the TS is approached, the closed-shell σ_{OO} orbital gradually splits into up- and down-spin orbitals ($\psi^{\pm}$), which are more or less localized on the terminal oxygen atoms, rather than concentrated in the same region of space. This is responsible for a homolytic diradical character, which is calculated to be 11.1% diradical at the TS ($\omega = 26.2°$, $n_{HONO} = 1.61$, $n_{LUNO} = 0.39$), relative to the pure diradical state, an extreme limit without atomic overlap ($\omega = 45°$, $n_{HONO} = n_{LUNO} = 1.0$). As shown previously, such an orbital-symmetry breaking is responsible for a high probability of spin transition from the singlet state to a triplet state,[28] whose potential surface cuts through the singlet surface in the vicinity of the TS (Figure S1A, Supporting Information).

The two monoanion states, $(O_XH, N_1H, O_Y)^-$ and $(O_X, N_1H, O_YH)^-$, in which either one of the two phenolic OH groups is deprotonated, behave in an entirely different manner. The highest occupied orbital is now switched from the σ_{OO} orbital in the neutral state to the π_{PhO} orbital of relative high energy in the monoanion state that spreads over the electron-rich phenoxide anion group, while the lowest unoccupied orbital remains the σ_{OO}* orbital; compare Figure 3D,E with Figure 3A. Contrary to the case of the neutral state, a pair of electrons that occupies the π_{PhO} orbital does not rise up along the O−O bond dissociation but rather falls steadily to a bonding level due to the interaction of the π_{PhO} orbital with the descending σ_{OO}* orbital; therefore, the reaction is essentially symmetry allowed. Owing to the intramolecular charge-transfer (CT) interaction, the HONO and LUNO become $(1 - \alpha^2)^{1/2}\pi_{PhO} + \alpha\sigma_{OO}$* and $-\alpha\pi_{PhO} + (1 - \alpha^2)^{1/2}\sigma_{OO}$*, in which the parameter α means that the NOs are not equally weighted on both sides but rather are dependent on the position along the reaction coordinate. As the reaction proceeds, a pseudo $((1 - \alpha^2)^{1/2}\pi_{PhO} + \alpha\sigma_{OO}^*)^2 \rightarrow (-\alpha\pi_{PhO} + (1 - \alpha^2)^{1/2}\sigma_{OO}^*)^2$ CT excitation is also promoted by the electron−electron repulsion so as to lower the energy of the ground-state wave function as much as possible, as shown in eq 4.

$$\psi^{\pm} = \cos\omega(\sqrt{1 - \alpha^2}\,\pi_{PhO} + \alpha\sigma_{00}^*) \pm \sin\omega(-\alpha\pi_{PhO} + \sqrt{1 - \alpha^2}\,\sigma_{00}^*) \quad (4)$$

The occupation of the LUNO ($\omega \rightarrow 45°$), which has a larger weight on σ_{OO}*, triggers a further O−O bond dissociation and a stronger CT interaction ($\alpha \rightarrow 1/\sqrt{2}$); $\psi^{\pm} = \pi_{PhO}$ ($\omega = 0°$, $\alpha = 0$) at the equilibrium geometry, while $\psi^{+} \approx \sigma_{OO}$* and $\psi^{-} \approx \pi_{PhO}$ ($\omega \approx 45°$, $\alpha \approx 1/\sqrt{2}$) at a sufficiently O−O cleaved structure. Thus, up-spin density emerges on the dissociating peroxide bond, while down-spin density on the electron-donating substituent, which shows a CT diradical character. The CT diradical TSs are located to be very early ($r_{OO}^{\ddagger} = 1.63$−1.65 Å, $y^{\ddagger} = 0.2$−0.4%), as compared with the homolytic diradical TS in the neutral state ($r_{OO}^{\ddagger} = 1.99$ Å, $y^{\ddagger} = 11.1$%), since the highest occupied π_{PhO} orbital lies close to the σ_{OO}* orbital, and accordingly, the activation barriers are considerably lowered (1.5 kcal mol^{-1}). Such an orbital-symmetry switch from forbidden radical (FR) in eq 3 to allowed radical (AR) in eq 4 mediated by the CT interaction has the benefits of not only activating the O−O bond but also avoiding unfavorable intersystem crossing,[28] even though a surface crossing appears between singlet and triplet states along the reaction pathway (Figure S1D,E, Supporting Information).

Puzzling results arise from the monoanion state with an amido anion electron donor, $(O_XH, N_1, O_YH)^-$. Two possibilities exist

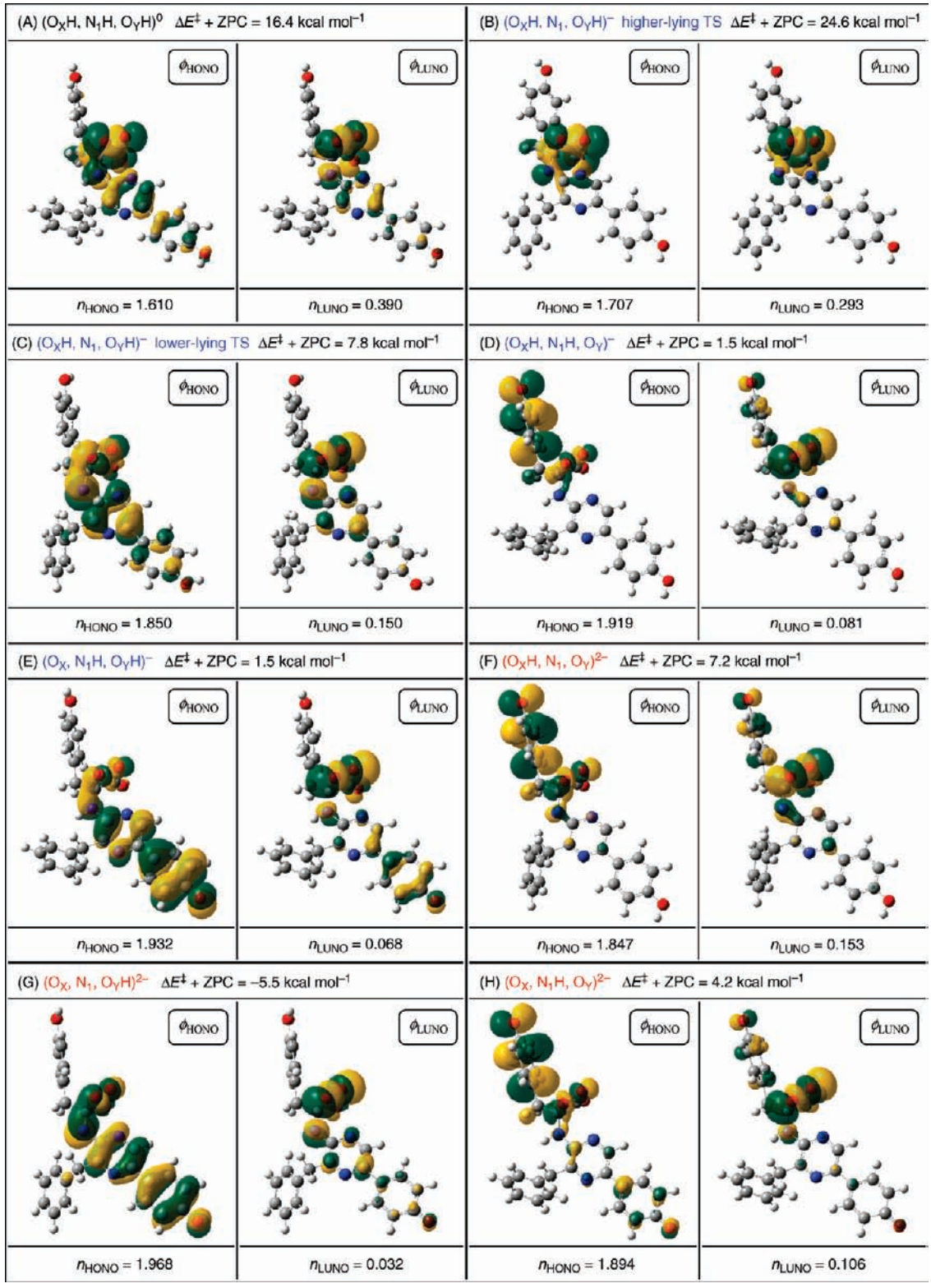

Figure 3. Highest occupied (ϕ_{HONO}) and lowest unoccupied (ϕ_{LUNO}) natural orbitals and their occupation numbers (n_{HONO} and n_{LUNO}) at TSs for the thermolysis of isolated dioxetanones $\mathbf{3}^z$, at the B3LYP/6-31+G(d) level.

in the presence of two lone pairs at the nitrogen atom, one being in a vertical pπ orbital and the other a horizontal sp^2 orbital.[31] We found a TS for decomposition that lies 24.6 kcal mol^{-1} higher than the dioxetanone intermediate, $\mathbf{3}^-$ $(O_XH, N_1, O_YH)^-$. Salient geometrical features of this TS are a short C_3-C_4 bond length (1.607 Å), tetrahedral binding of the C_3 atom (dihedral angle $O_\beta C_3 C_2 O_\gamma$ is 128.9°), and a significant O−O bond distance (1.935 Å), as indicated in the top of Figure 4. The reason for these features is that the interaction of the σ_{N1} orbital with the symmetric combination of the nitrogen lone pairs of the pyrazine ring pushes up the latter so that the pyrazine moiety becomes a somewhat poorer leaving group.[32] The amplitude patterns of HONO and LUNO at the TS are symmetric and antisymmetric with respect to a local symmetry plane that cuts through the O−O bond, as shown in Figure 3B, which indicates a homolytic diradical character. We could also locate another TS that lies

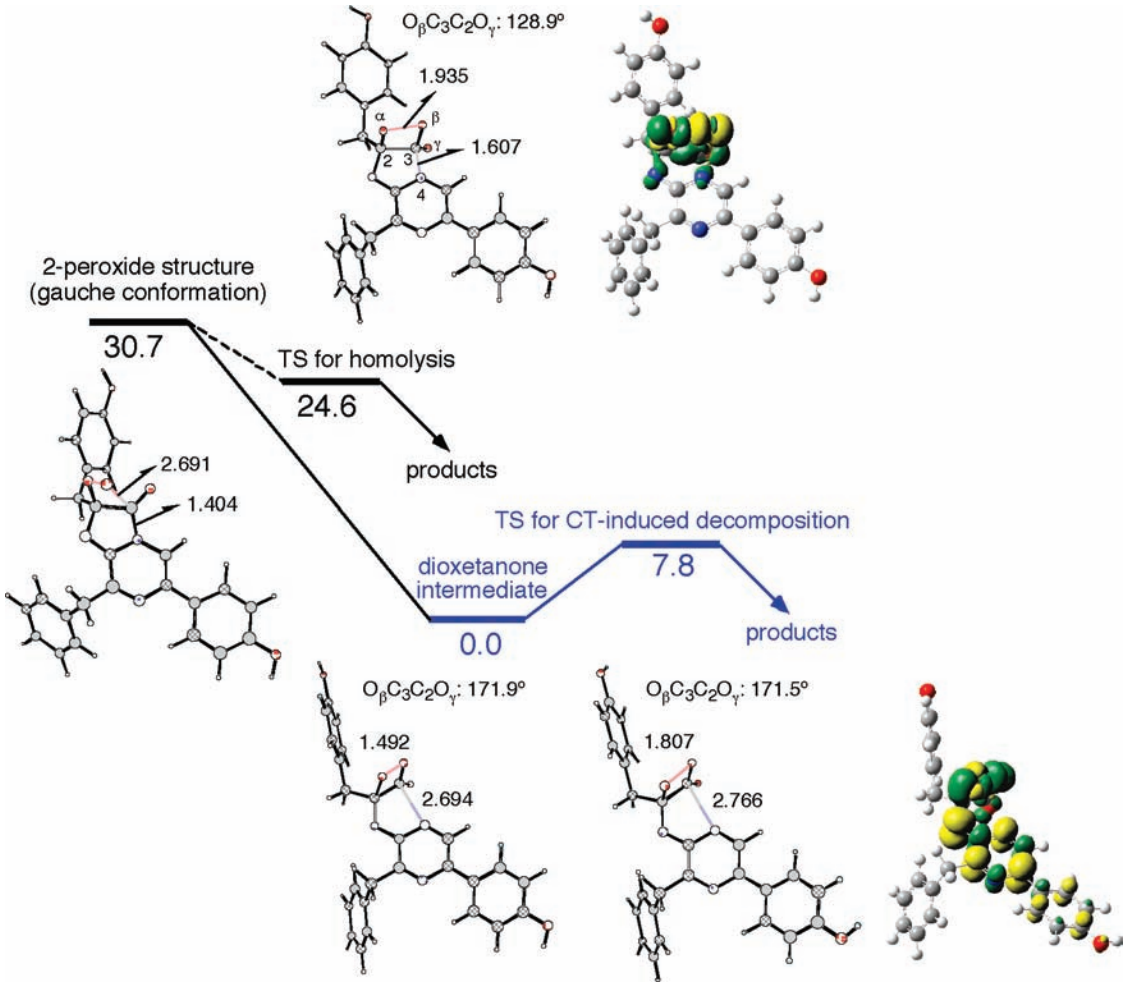

Figure 4. Energy profile for the thermolysis of isolated dioxetanone $\mathbf{3}^-$ $(O_XH, N_1, O_YH)^-$, at the B3LYP/6-31+G(d) level. Relative energies including ZPC are given in kcal mol^{-1}. Bond lengths are given in angstroms. Spin density distributions at TSs are depicted with up and down spins colored green and yellow.

7.8 kcal mol^{-1} above the dioxetanone intermediate but well below the homolytic diradical TS, as displayed in the bottom right of Figure 4. At this TS, the C_3-C_4 bond is completely cleaved (2.766 Å) and the O−O elongation is relatively slight (1.807 Å), as compared with the homolytic diradical TS. HONO and LUNO at this lower-lying TS, as shown in Figure 3C, clearly indicate that the relatively low barrier for decomposition is a result of the intramolecular CT interaction of the π_{N1} orbital, which is delocalized into the pyrazine ring, with the σ_{OO}* orbital. The distinct features of the two TSs can also be seen from the spin density distributions (Figure 4); spin density is localized on the dissociating peroxide bond at the higher lying TS, while down-spin density (yellow) is delocalized over the pyrazylamine ring at the lower-lying TS. Static calculations cannot determine the branching ratio between the homolytic and CT diradical pathways, both of which are energetically accessible from the precursor 2-peroxide structure (Figure 4).[33] However, it is reasonable to suppose that most trajectories will lead first to the formation of the dioxetanone intermediate; i.e., the C_3-C_4 bond breaking will be preferred over the homolytic O−O dissociation because of a stronger thermodynamic driving force for the former. Once the C_3-C_4 bond has been cleaved completely, a barrier of 24.6 kcal mol^{-1} has to be overcome for homolysis, i.e., 16.8 kcal mol^{-1} higher than that for CT-induced decomposition. We should also mention that the HONO at the lower-lying CT diradical TS has a significant magnitude of coefficient in the p orbital of the O_α atom perpendicular to the approximate plane of the dioxetanone skeleton (Figure 3C), which suggests that the spin transition at the S_0/T_1 crossing seam is not negligible, as mentioned previously.[28]

Irregular results originate from the dianion state, $(O_X, N_1, O_YH)^{2-}$, in which the two negative charges (amido anion and phenoxide anion) are present on the same side of two substituents attached to the dioxetanone functionality. In this case, an open-chain 3-peroxide intermediate becomes much more stable (by 11.9 kcal mol^{-1}) than the cyclic dioxetanone structure, as shown in Figure 5; note that a shallow minimum (by 0.4 kcal mol^{-1}) for the cyclic dioxetanone structure disappears with the inclusion of ZPC. This is due to the strong resonance stabilization of the highly conjugated system,[34] which largely accounts for an appreciable activation barrier of 6.4 kcal mol^{-1} for the CT-induced decomposition. The fact that the decomposition reaction is attended by a significant C_3-N_4 bond elongation makes skipping over the 3-peroxide intermediate unlikely.

The other two doubly deprotonated states, $(O_XH, N_1, O_Y)^{2-}$ and $(O_X, N_1H, O_Y)^{2-}$, differ from the $(O_X, N_1, O_YH)^{2-}$ dianion state mentioned above, in that the former two species has two monoanionic substituents at the geminal positions of the dioxetanone functionality. This difference is reflected in the fact that, in the former two cases, there exists a well-defined dioxetanone intermediate on the potential surface. The activation barriers for the CT-induced decomposition of the cyclic dioxetanone intermediates are appreciable, 7.2 and 4.2 kcal mol^{-1} for the $(O_XH, N_1, O_Y)^{2-}$ and $(O_X, N_1H, O_Y)^{2-}$ states (Table 1).

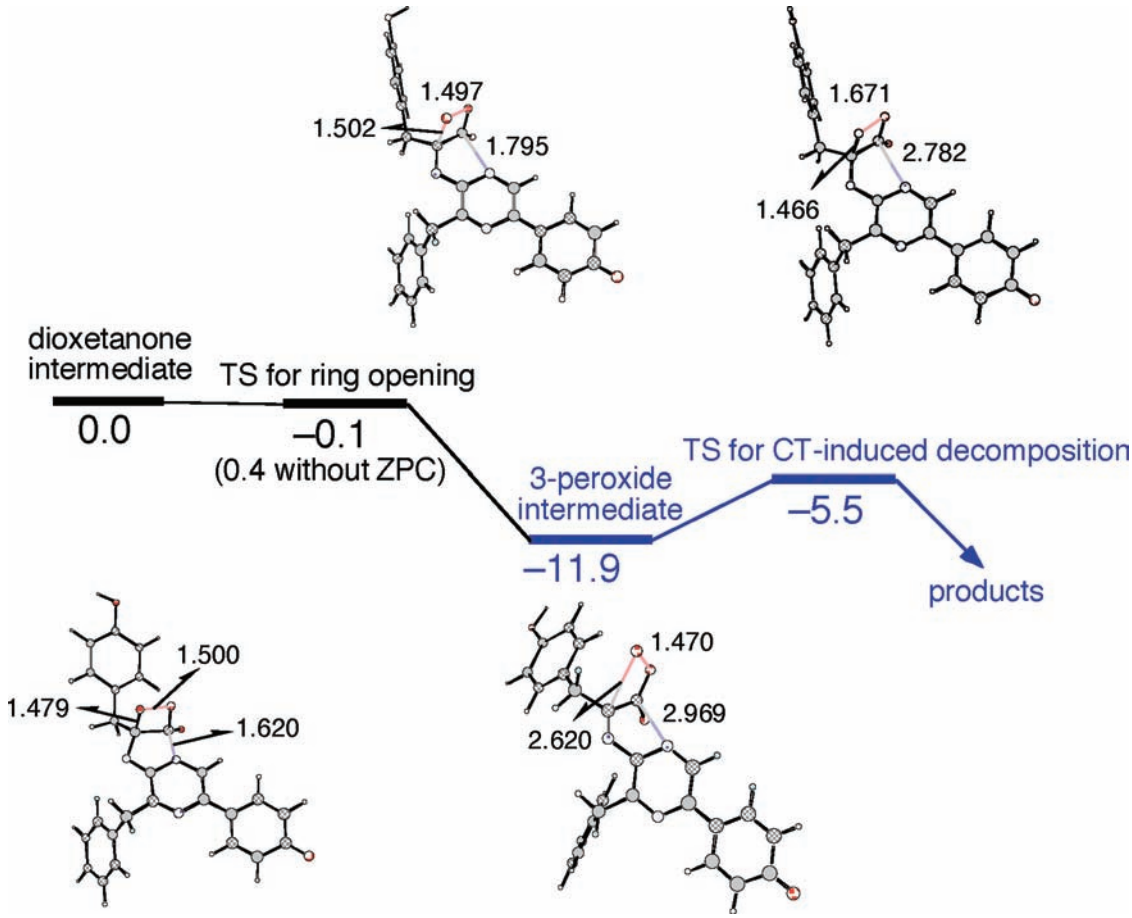

Figure 5. Energy profile for the thermolysis of isolated dioxetanone $\mathbf{3}^{2-}$ $(O_X, N_1, O_YH)^{2-}$, at the B3LYP/6-31+G(d) level. Relative energies including ZPC are given in kcal mol^{-1}. Bond lengths are given in angstroms.

The natural orbital analyses of the CT diradical TSs reveal that the phenoxide anion group at the C_{10} position, rather than the amido anion group or the phenoxide anion group at C_6 position, acts as an electron donor (Figure 3F,H).

In the trianion state, $(O_X, N_1, O_Y)^{3-}$, in which all three titratable sites are deprotonated, the electron-donor part is now switched to the combined part of the amido anion group and the phenoxide anion group at C_6 position, similarly to the case of $(O_X, N_1, O_YH)^{2-}$. CT-induced decomposition occurs via a cyclic dioxetanone intermediate with an activation barrier of 5.4 kcal mol^{-1}.

The reflection on the foregoing analyses could provide some insight into the important factors that may affect the singlet excitation efficiency in chemi- and bioluminescence. In the neutral state, $(O_XH, N_1H, O_YH)^0$, and the amido anion state, $(O_XH, N_1, O_YH)^-$, the problem on the spin-transition phenomenon, i.e., a decay process to the lower-lying triplet state, cannot be neglected for the consideration of the singlet excitation efficiency in the thermolysis of peroxidized coelenterazine. Additional insight is provided by constraint geometry optimizations including solvent correction with the O−O bond length fixed at the one for the TS in the gas phase. The converged spin density distributions of the neutral species $(O_XH, N_1H, O_YH)^0$ are placed in Figure 6 in order of increasing solvent polarity. The results clearly indicate that a polarizing medium effect affects the electronic mechanism (in favor of the CT diradical mechanism) for the neutral system.[35] The reason for this mechanistic change from homolysis in the gas phase to CT-induced decomposition in acetonitrile and benzene is that the spatial separation between the potent electron donor (4-hydroxyphenyl group at the C_6 position) and the acceptor (the dissociating peroxide bond) can create a large dipole moment by an intramolecular CT, which should be well solvated by a surrounding polarizing medium. In fact, the dipole moment (μ) at the TS is calculated to be 7.1 D in the gas phase, while it increases to 22.2 (15.2) D at a relaxed geometry in acetonitrile (benzene), as indicated in Figure 6. This finding as well as experimental observation of substituent effects in neutral systems[36] are indicative of the operation of the CT diradical mechanism in an organic solvent.

We may safely say that, in two monoanion states with a phenoxide anion group, $(O_XH, N_1H, O_Y)^-$ and $(O_X, N_1H, O_YH)^-$, the spin symmetry is much more conserved than in the neutral and amido anion states. The predominant factor determining the singlet excitation efficiency will be related to the nonadiabatic process for a $S_0 \rightarrow S_1$ excitation, which is, however, the most difficult part to understand. Two major mechanisms have so far been suggested: a concerted one associated with a conical intersection or a weakly avoided crossing[34,37] and a stepwise one via an effectively caged radical pair.[38,39] We believe that the high-efficiency chemiluminescence reactions of synthetic compounds (e.g., peroxides with an odd-patterned fluorophore) should be concerted not stepwise.[40] An illustrative example is provided by the efficient light-harvesting ability of dendrimers, which create an exciton funnel from its periphery to a focal point via *meta*-substituted benzene rings.[41] A lot of experimental results on synthetic dioxetane systems has also been interpreted in terms of the concerted mechanism.[42]

The situation may be quite confused in biological systems because of the presence of relatively strong thermodynamic

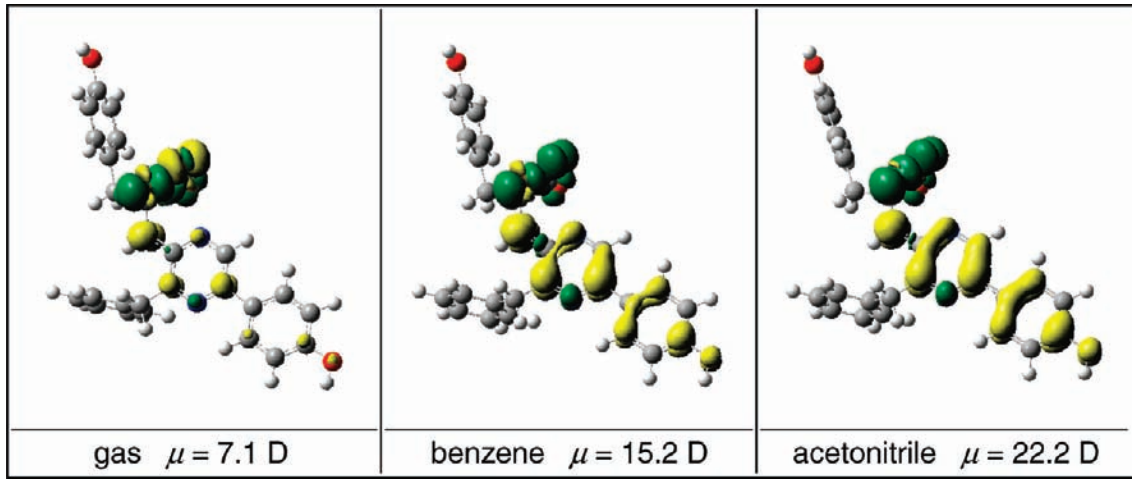

Figure 6. Spin density distributions of dissociating dioxetanone **3** (O_XH, N_1H, O_YH)^0 ($r_{OO} = 2.0$ Å), at the CPCM B3LYP/6-31+G(d) level [$\varepsilon = 2.247$ (benzene) and 36.64 (acetonitrile)]. Up and down spins are green and yellow. Dipole moments (μ) are given in Debye.

driving force for the electron-transfer reaction leading directly to $\mathbf{4}^{\bullet(z+1)}$ and $CO_2^{\bullet-}$ that is energetically in competition with other reaction pathways.[43] Care should be required, since the primary products are not uniquely defined in static calculations. The driving forces for the neutral and monoanion states, in particular, increase further in a polarizing medium, while it decreases in the case of dianionic species.[43] These results led us to a hypothesis of mechanistic dichotomy in charge-transfer-induced luminescence (CTIL) that involves competing concerted and stepwise excitation processes mediated by a CO_2 vending vibration and by a solvent polarity.[40] Both concerted and stepwise mechanisms can potentially explain the three- or four-digit enhancement of bioluminescence efficiency. The concerted process for bioluminescence activity can be properly expressed by the term "entatic state" for the function of enzymes,[44] in the sense that a steric constrant imposed by protein inevitably distorts a substrate geometry so that most reaction trajectories are forced to reach a region of conical intersection.[45] In contrast, the term "confined state"[46] may be appropriate for the stepwise process, in which a slightly separated $CO_2^{\bullet-}$ may be momentarily attached to residues in the protein pocket (most probably protonated His169)[47] and may have a chance to experience a subsequent back electron transfer between transient radicals with a lifetime that may be closely coupled with the symmetric bending vibration mode of CO_2. In such a case, the excitation probability should be dependent on electronic coupling matrix elements and hence on the spatial distributions of the SOMO and LUMO of a substrate radical as well as the position of $CO_2^{\bullet-}$. This stepwise reaction may be rather similar to the multistep electron transfer in photosystem II.[48] At present, a full theoretical description of the excitation mechanism operating within aequorin is an extremely difficult and complicated task, since the partitioning between the different possible mechanisms is essentially a problem of dynamics. Future elaborate simulations for protein dynamics are obviously needed to verify whether the above "scenarios" can be operative in aequorin or should be discarded. We are currently working out the plan in a stepwise manner. In the next subsection, we shall focus on the topics that are inherently important whatever the excitation mechanism should turn out to be.

3.2. Influence of Hydrogen-Bond Interactions on the Thermal Decomposition of Peroxidized Coelenterazine. As a second part of this study, we have studied some external perturbations caused by hydrogen bonding and polarizing medium effects to an isolated peroxidized coelenterazine. This examination is of considerable interest in terms of the regiochemistry in the oxidation of coelenterazine **1H** by O_2 and the pK_a regulation of a peroxidized substrate for the preferential generation of primary oxidation products in a singlet state. The regiochemistry problem arises from the fact that dioxetanone ($\mathbf{3}^z$) and dioxetane ($\mathbf{6}^z$) intermediates are generated from the competitive attack of O_2 on the C_2 and C_5 positions of coelenterazine (**1H** or $\mathbf{1}^-$),[49] as shown in Scheme 2. As reported previously for the thermolysis of phenoxide-anion-substituted dioxetanes and dioxetanones with the anion site hydrogen-bonded to one, two, or three water molecules,[50,51] the dioxetane functionality is highly susceptible to the change in charge and spin distributions during its decomposition via hydrogen bonds, thereby leading to relative strong and variable SOC between low-lying singlet and triplet states (5.3−95 cm^{-1}), while this is not the case when the dioxetanone functionality is present (0.2−0.3 cm^{-1});[50] i.e., the dioxetanone functionality is inherently important to the suppression of unfavorable intersystem crossing in the product formation. These results have a potential significance to bioluminescence, since the X-ray crystallography study of aequorin has revealed that a peroxidized coelenterazine is buried at a hydrophobic core cavity isolated from solvent and is hydrogen bonded to surrounding amino acid residues without any covalent bonds.[9]

There are three characteristic Tyr-His-Trp triad motifs at around the coelenterazine-binding site of aequorin,[9] which may serve as one of the driving forces in molecular recognition; the histidine and tyrosine residues make three pairs, each being closely associated with a tryptophan. Considerations of the roles of these triads may offer the key to an understanding of the bioluminescence activity.[9] We have examined herein the direct influence of the electrostatic interactions caused by the triad Tyr82-His16-Trp86 located near the phenol/phenoxide anion group attached at the C_6 position of coelenterazine. The investigation of this triad is illuminating, whatever part of the protein environment is omitted initially, since the deprotonation of the phenolic OH group of the neutral substrate realizes the monoanion state (O_X, N_1H, O_YH)$^-$, which is a favorable condition for the conservation of spin symmetry if the substrate is in an isolated system.[28] His16 is the most likely a receptor for the proton, forming a local ion pair. We have constructed simple model complexes that consist of a dioxetane ($\mathbf{6}^-$) or dioxetanone ($\mathbf{3}^-$) substrate with the protonation state of (O_X, N_1H, O_YH)$^-$ and three model molecules of amino acid residues, in which protonated histidine, tyrosine, and tryptophan residues

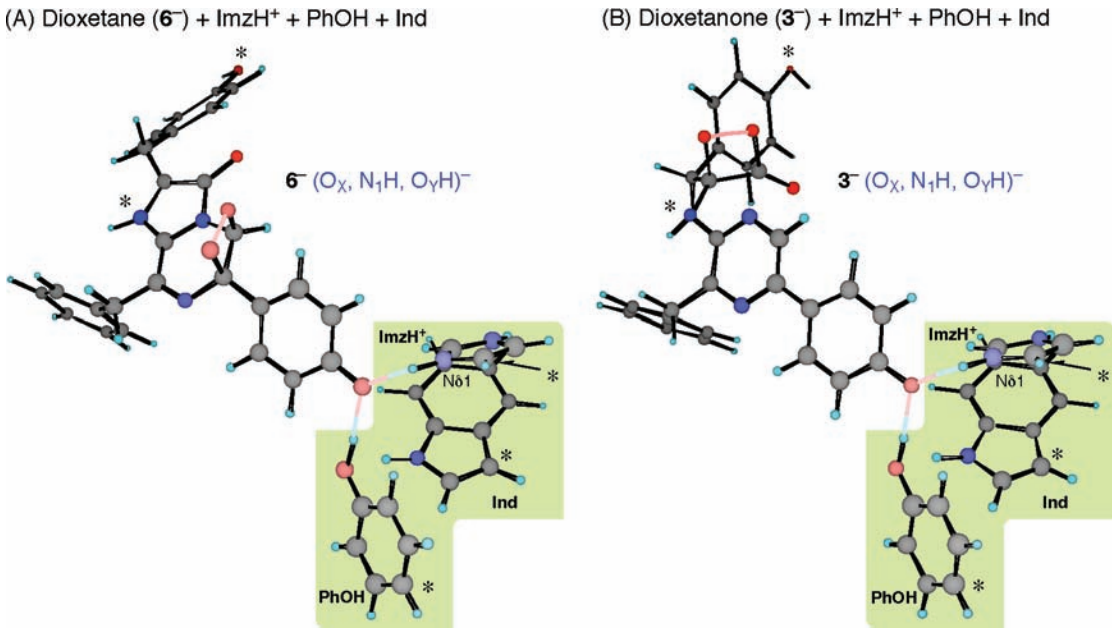

Figure 7. Model complexes for the coelenterazine-biding site of aequorin. Tyr82, His16, and Trp86 are modeled as phenol (PhOH), imidazolium cation ($ImzH^+$), and indole (Ind). Atoms marked with an asterisk are kept frozen in geometry optimizations.

SCHEME 2

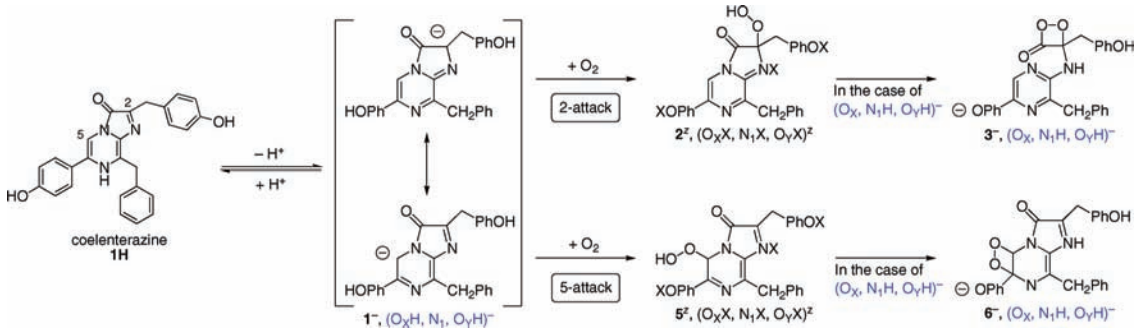

are modeled as imidazolium cation ($ImzH^+$), phenol (PhOH), and indole (Ind), as displayed in Figure 7. The total charge of the model systems is set to be zero. An important assumption of our models is that these residues have, to some extent, hydrogen bonding with the peroxide anion even in the presence of a fluctuation of the protein triggered by Ca^{2+} binding. We have considered only the phenoxide monoanion species of $\mathbf{6}^-$ and $\mathbf{3}^-$ and their relevant protonation states, which may be generated thermodynamically as judged from the proton affinities of the peroxides.[52] At the present stage, however, the involvement of the amido monoanion spices and the dianion species cannot be entirely ruled out and has to be examined carefully in a future study. We performed constraint geometry optimizations at the B3LYP/6-31G(d) level with the peroxide O−O bond length fixed at a certain value to obtain minimum-energy paths (MEP). To mimic steric constraints exerted by the protein environment, atoms marked with an asterisk, which are directly connected to the backbone or hydrogen bonded to the side chain of an amino acid residue, are fixed to their X-ray position (1EJ3).[9] For the system containing $\mathbf{3}^-$, the Nδ1-H bond of imidazolium is also kept frozen at 1.015 Å to prevent spontaneous proton transfer (see discussion later). Single-point solvent calculations were carried out with the CPCM-UAKS model using a dielectric of 4.0 to simulate a hydrophobic environment of a protein interior.

Barrier heights for the thermolysis of the dioxetane ($\mathbf{6}^-$) and dioxetanone ($\mathbf{3}^-$) intermediates [$(O_X, N_1H, O_YH)^-$] interacting with three model residues, PhOH, $ImzH^+$, and Ind, are roughly estimated to be 17.8 and 12.3 kcal mol^{-1} with thermal contribution omitted. These values are taken from the relative energies of maximum points (r_{OO} = 1.88 and 1.80 Å) along the MEPs for the thermolysis of $\mathbf{6}^-$ and $\mathbf{3}^-$, as shown in Figure 8. These values are much larger than those of isolated peroxides (4.2 and 1.5 kcal mol^{-1} with ZPC for $\mathbf{6}^-$ and $\mathbf{3}^-$) because of constraint geometry optimizations and electrostatic interaction between the anion site of the peroxide and $ImzH^+$ that stabilizes the negative charge on the oxidophenyl group of the peroxide. In each case, singlet and triplet states cross along the MEP (Figure 8). A closer look of the potential curves indicates a difference between $\mathbf{6}^-$ and $\mathbf{3}^-$. In $\mathbf{6}^-$, there is a discontinuity along the MEP at around r_{OO} = 1.93 Å, as specified by an arrow in Figure 8A, while the curve is continuous and smooth in $\mathbf{3}^-$ (Figure 8B). This discontinuity cannot be resolved by our procedure for obtaining the MEPs with one variable, r_{OO}.

To understand the physical reason for the discontinuity, we depict in Figure 9A, the distributions of spin density of $\mathbf{6}^-$ before and after the discontinuity point (r_{OO} = 1.9 and 2.0 Å). At r_{OO} = 1.9 Å, the up (green) and down (yellow) spin densities are localized on the pσ orbitals of the terminal oxygen atoms of the dissociating peroxide bond. This is a typical feature of the

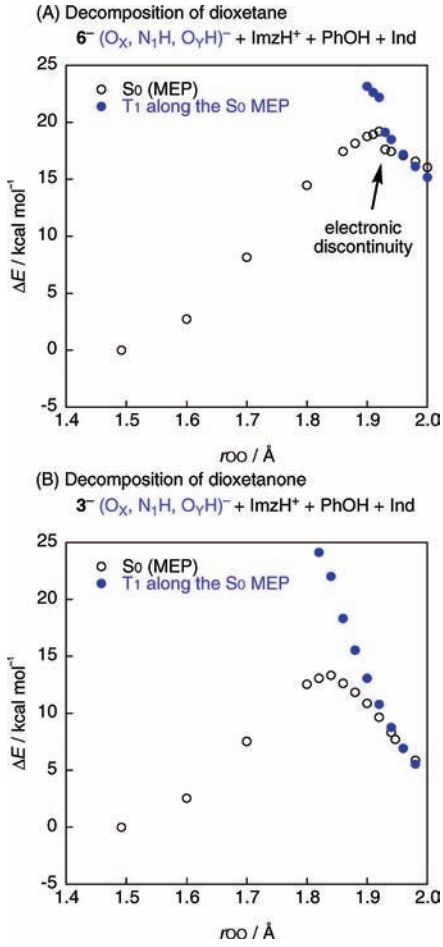

Figure 8. Energy profiles of minimum-energy paths (MEP) (black circles) and T_1 energy changes along the MEPs (blue circles) as a function of the O−O bond distance (r_{OO}) for the thermolysis of dioxetane ($\mathbf{6}^-$, A) and dioxetanone ($\mathbf{3}^-$, B) with PhOH, $ImzH^+$, and Ind, at the CPCM B3LYP/6-31G(d) level ($\varepsilon = 4.0$).

homolytic diradical mechanism, which we call here $^1\sigma\sigma$. At $r_{OO} = 2.0$ Å, however, the down-spin density becomes delocalized over the substituent. This means that the sufficiently dissociated dioxetane exhibits a CT diradical character, which we call here $^1h\sigma$. The thermolysis of dioxetane $\mathbf{6}^-$ is, therefore, regarded as an illustrative example of reactions that fall into an intermediate between the homolytic and CT diradical mechanisms.[53] This feature is common to the thermolysis of phenoxide-anion-substituted dioxetanes having one or two water molecule(s) at the anion site (Table S3, Supporting Information).[50] The fact that the different sets of orbitals that unpaired electrons occupy cannot be smoothly correlated with each other[54] is the origin of the discontinuity appearing on the group-state MEP. In the short region between the homolytic and CT diradical surfaces, the appropriate state should be described as a resonance, $^1\sigma\sigma \leftrightarrow {}^1h\sigma$; i.e., heavy configuration interaction should occur. The in-phase and out-of-phase combinations of the resonance contributors imply that there should be a second singlet state and a second triplet state that lie slightly above the singlet and triplet ground states. The dissociating dioxetane on the ground-state surface may cross to the lowest excited states. We now draw attention to the spin density distribution for the CT diradical state of $\mathbf{6}^-$ ($r_{OO} = 2.0$ Å), which shows that the down-spin unpaired electron also contributes to the p-type orbital of the oxygen atom of the peroxide bond that is perpendicular to the approximate plane of the dioxetane skeleton[55] (the right-hand side of Figure 9A). This means that the CT diradical state of $\mathbf{6}^-$ actually borrows somewhat form a $^1n\sigma$ character. We can predict that, among the four configurations, the cross couplings between singlet and triplet configurations of different spatial characteristics, $^1\sigma\sigma \leftrightarrow {}^3h\sigma$ ($\sim {}^3n\sigma$) and $^3\sigma\sigma \leftrightarrow {}^1h\sigma$ ($\sim {}^1n\sigma$), should be strong, since a change in orbital angular momentum can create a torque capable of flipping electron spin.[28]

The left-hand side of Figure 9B depicts spin density distribution of dissociating dioxetanone $\mathbf{3}^-$ at $r_{OO} = 2.0$ Å. The result clearly indicates that $\mathbf{3}^-$ decomposes by a successive O−O dissociation through the CT diradical mechanism, since down-spin density is essentially localized on the substituent and up-spin on the dissociating peroxide bond. Contrary to the case of dioxetane $\mathbf{6}^-$, the penetration of down-spin density into the peroxide bond is negligible. The coupling between closely lying singlet and triplet ground states with a similar electronic configuration labeled, $^{1,3}h\sigma$, should be weak. The reason for the difference between dioxetane $\mathbf{6}^-$ and dioxetanone $\mathbf{3}^-$ can be attributed to the fact that the dioxetanone structure is inherently a much better electron acceptor than the dioxetane structure;[40] the vertical electron affinity of unsubstituted dioxetanone is significant [−0.4 eV (equilibrium) and ca. 3.6 eV ($r_{OO} > 2.0$ Å)], as compared with unsubstituted dioxetane [−1.1 eV (equilibrium) and ca. 2.4 eV ($r_{OO} > 2.0$ Å)].

This finding highlights the importance of regiochemical control by external hydrogen-bond interactions with Tyr184 and His169 in the hydrophobic binding cavity of aequorin, as revealed by the X-ray structure (Figure 1).[9] There are no such residues capable of forming a hydrogen-bond network near the C_5 position of coelenterazine. The importance becomes apparent if we examine the energetics of hydroperoxde species, **2** and **5** (Scheme 2), in organic solvents (Tables S4 and S5, Supporting Information). If the substrate is in its deprotonated form, $\mathbf{1}^-$, the dioxetanone functionality can be established at the expense of an extra energy required for the formation of a coelenterazine−2-hydroperoxide adduct **2**, which lies above its regioisomer 5-hydroperoxde species **5** by ca. 2−3 kcal mol^{-1} for $(O_XH, N_1, O_YH)^0$ and ca. 10−17 kcal mol^{-1} for $(O_X, N_1H, O_YH)^0$ except for $(O_XH, N_1H, O_Y)^0$ (nearly thermoneutral in benzene).[56]

In what follows, we shall concentrate on the thermolysis of dioxetanone $\mathbf{3}^z$. If the proton attached to the Nδ1 atom of imidazole in the dioxetanone system ($\mathbf{3}^- + ImzH^+ + PhOH + Ind$) is allowed to change its position during geometry optimization, it spontaneously moves from the Nδ1 position to the oxido anion moiety of $\mathbf{3}^-$; accordingly, the protonation state of the peroxide is converted into the neutral state, **3** $(O_XH, N_1H, O_YH)^0$, which lies much below (by 9.8 kcal mol^{-1}) the monoanion state $\mathbf{3}^-$ $(O_X, N_1H, O_YH)^-$. This automatic proton transfer provokes a profound influence on the decomposition mechanism. The barrier height for **3** is estimated to be 17.8 kcal mol^{-1}, as a maximum ($r_{OO} = 1.92$ Å) along the MEP for the O−O bond dissociation (Figure S6, Supporting Information), which is 4.4 kcal mol^{-1} higher than that for $\mathbf{3}^-$. As shown in the right-hand side of Figure 9B, the spin density becomes mostly located on the dissociating peroxide bond, as does in the early stage of the thermolysis of dioxetanes $\mathbf{6}^-$ (the left-hand side of Figure 9A). We should, therefore, notice a variable TS or two competing pathways available in the product formation, which correspond to the homolytic and CT diradical mechanisms.

It is interesting to investigate how the orbital characteristics is affected if the proton migrates from the oxido (O_X) moiety of $\mathbf{3}^-$ to the Nδ1 atom of Imz or conversely during the decomposition of dioxetanone, **3** $(O_XH, N_1H, O_YH)^0$ or $\mathbf{3}^-$ $(O_X, N_1H, O_YH)^-$. Figure 10A demonstrates the plots of energy

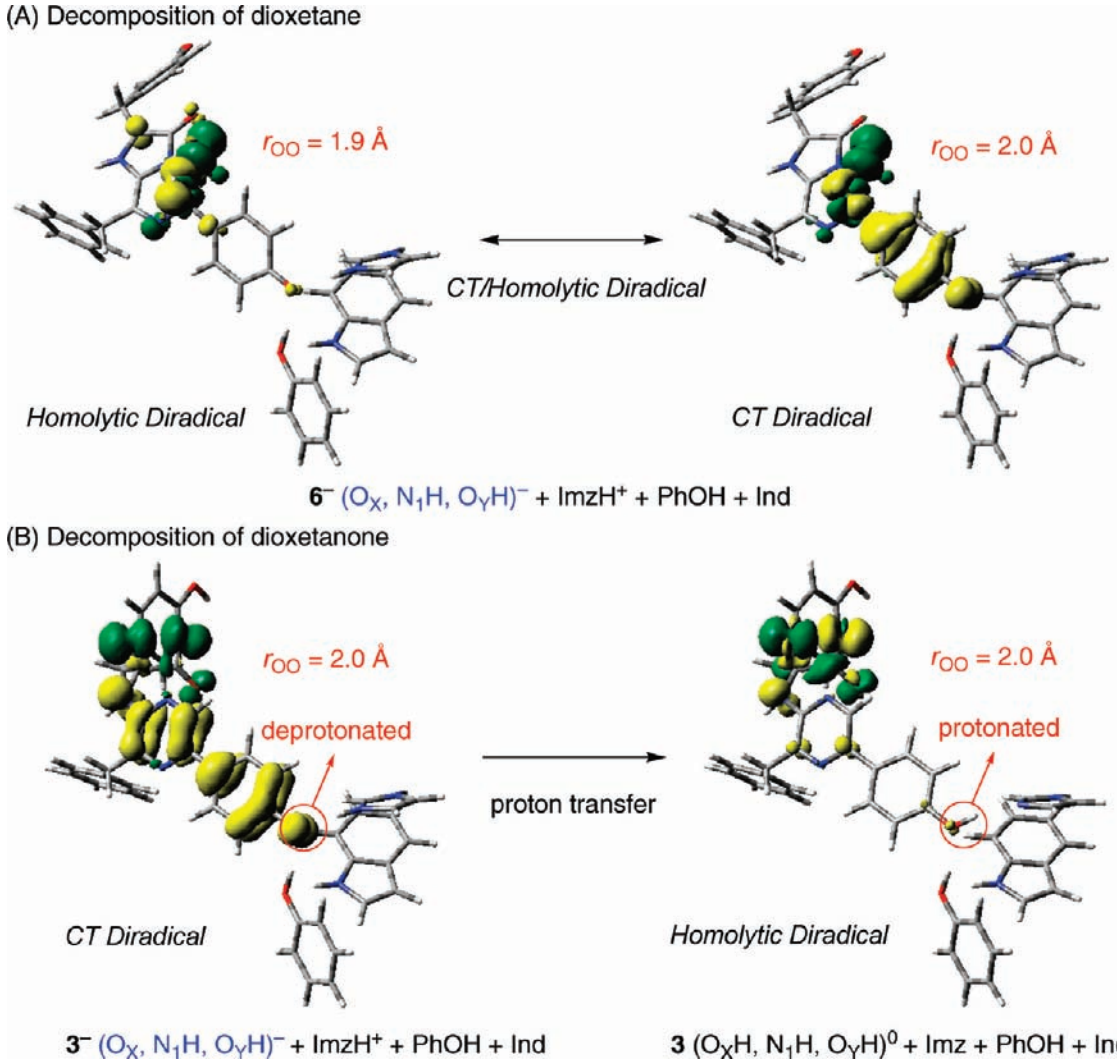

Figure 9. Spin density distributions of dissociating peroxides with PhOH, $ImzH^+$, and Ind, at the CPCM B3LYP/6-31G(d) level ($\varepsilon = 4.0$). Up and down spins are green and yellow.

change and spin density distributions along the proton exchange between $\mathbf{3}^-$ and Imz as a function of an index that measures the degree of deprotonation to the O_X position, $p \equiv r_{OxH}/(r_{OxH} + r_{N\delta 1H})$, in which r_{OxH} and $r_{N\delta 1H}$ are bond lengths defined in the top of Figure 10. The energies plotted in Figure 10A are determined by freezing the peroxide O−O bond (r_{OO}) at 2.0 Å and either r_{OxH} or $r_{N\delta 1H}$ at a different value and optimizing other degrees of freedom except for constraint imposed on atoms marked with an asterisk. We can see a small barrier on the potential surface with the maximum point ($p \approx 0.45$) being about 4.6 and 7.5 kcal mol^{-1} above **3** and $\mathbf{3}^-$. When the proton comes near to the O_X position (the left-hand side of Figure 10A), the decomposing dioxetanone behaves like a homolytic diradical species, since up- and down-spin densities are mostly contracted on the oxygen atoms of the dissociating peroxide bond. Immediately after the maximum has been surpassed, down-spin density (yellow) rapidly spreads out over the whole substituent (the right-hand side of Figure 10A). This expansion of down-spin density can be confirmed by a steep rise with a negative sign in the grouped spin densities on the oxidophenyl moiety (σ_{PhO}), as indicated in Figure 10B. This charge reorganization, starting from **3**, corresponds to an electron shift from the local HOMO of the substituent to the σ_{OO} orbital of the dissociating peroxide bond caused by an intersection or near intersection between the rising π_{PhO} orbital and the σ_{OO} orbital and leaves effectively a radical hole on the substituent. The orbital-intersection region is variable and dynamic, since the σ_{OO} orbital is affected by the O−O bond dissociation, while the π_{PhO} orbital is sensitive to interelectronic repulsion (the degree of protonation). The protonation/deprotonation process serves as a switch of the electronic property of the dissociating peroxide.

The results derived from our simple model suggest that, in terms of thermodynamic equilibrium, the dioxetanone intermediate exists exclusively in the neutral state $(O_XH, N_1H, O_YH)^0$, which lies 9.8 kcal mol^{-1} lower in energy than the monoanion state $(O_X, N_1H, O_YH)^-$, as shown in Figure 11. However, since the barrier height for decomposition is usually higher in the neutral state than in the monoanion state, we must consider kinetics-driven branches of two possible pathways. Provided that the proton transfer for the interconversion of $(O_X, N_1H, O_YH)^-$ to $(O_XH, N_1H, O_YH)^0$ occurs very fast, as compared with the decomposition of dioxetanone, all trajectories will go through a lower-lying TS. Thus, the energy difference between the CT and homolytic diradical TSs ($\Delta\Delta G^{\ddagger}_{CT\text{-}HD}$), as indicated in Figure 11, is an essential criterion that determines the CT versus homolytic diradical mechanisms and hence singlet and triplet product distributions.[57] If $\Delta\Delta G^{\ddagger}_{CT\text{-}HD}$ is positive, the dioxetanone will decompose through the homolytic bond breaking, with concomitant proton transfer. In this case, the CT diradical TS will not have any reactive capability. The reverse is true, if

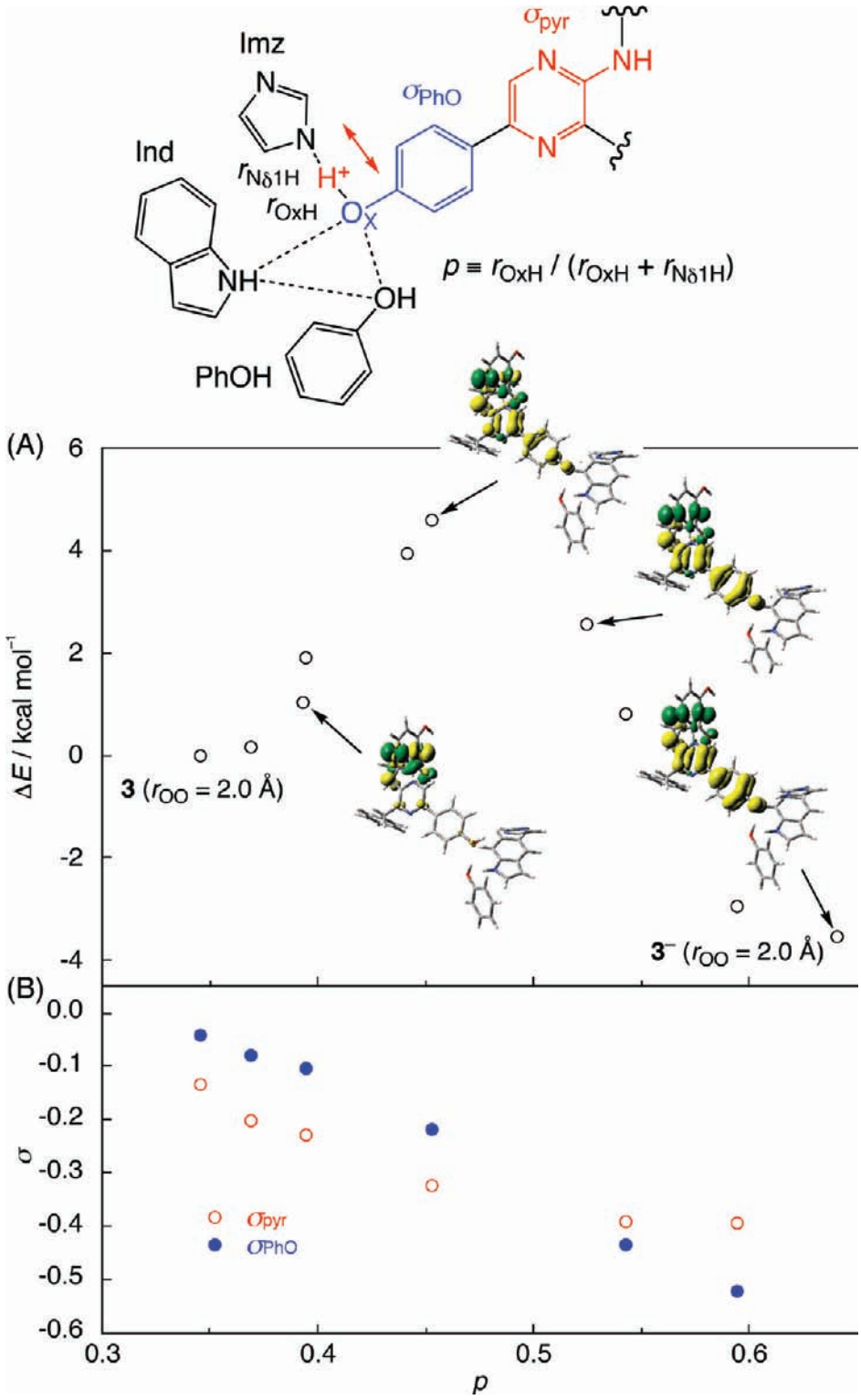

Figure 10. (A) Energy profile of minimum-energy path (MEP) as a function of the quantity p [$\equiv r_{OxH}/(r_{OxH} + r_{N\delta 1H})$] for the proton exchange between dissociating dioxetanone $\mathbf{3}^-$ [$r_{OO} = 2.0$ Å (fixed)] and Imz, at the CPCM B3LYP/6-31G(d) level ($\varepsilon = 4.0$). (B) Variations of grouped spin densities on the pyrazylamine (σ_{pyr}) and oxidophenyl (σ_{PhO}) moieties as a function of the quantity p.

$\Delta\Delta G^{\ddagger}_{CT\text{-}HD} < 0$, for which the CT diradical TS will participate in the reaction. Our model complex provides a positive value of $\Delta\Delta G^{\ddagger}_{CT\text{-}HD}$ (4.0 kcal mol^{-1}), which suggests that the decomposition reaction occurs by a homolytic O−O bond cleavage.

The apparent failure of our simple model complex to predict properly the CT diradical mechanism, through which primary products will be preferentially in a singlet state rather than a nonluminescent triplet state, implies that the size of the model complex as well as the procedure has to be extended to accommodate satisfactorily experimental facts. The conclusions deduced from the present model system have, of course, certain flexibilities in the exact interpretation of the processes in the actual biological system due to the rough approximation of surrounding protein by the polarizable continuum model. The discrepancy may be overcome in two different ways. The first important point for modifications is related with the pK_a

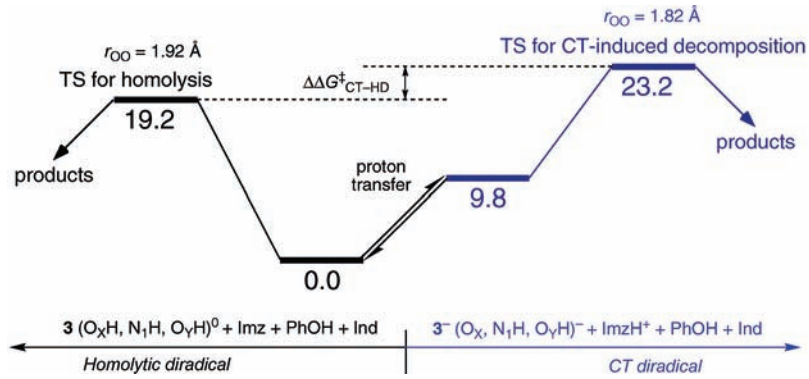

Figure 11. Energy profile for the thermolysis of dioxetanone **3**$^{\varepsilon}$ with PhOH, ImzH$^+$ (or Imz), and Ind, at the CPCM B3LYP/6-31G(d) level (ε = 4.0). Relative energies are given in kcal mol^{-1}.

regulation of the peroxide by residues located in the hydrophobic coelenterazine-binding site of aequorin. As mentioned above, the branching ratio of the CT to homolytic diradical pathways is determined only by the quantity, $\Delta\Delta G^{\ddagger}_{CT\text{-}HD}$, not by the relative stabilities of the protonation states of the intermediate **3**$^{\varepsilon}$. Thus, a slight pK_a reduction of the substrate (only by 4.0 kcal mol^{-1} in this case) is sufficient enough to change the sign of $\Delta\Delta G^{\ddagger}_{CT\text{-}HD}$ such that the CT-induced luminescence predominates, even though the neutral state is much more populated in the intermediate region of **3**$^{\varepsilon}$. It is, of course, not possible within the present model to estimate accurately the energetics of the proton transfer occurring between **3**$^{\varepsilon}$ and Imz in aequorin. Nevertheless, at present, it is worthwhile to mention that the Tyr-His-Trp triad motif has already an effect that reduces the proton affinity of the substrate; the endothermicity for the proton-exchange reaction between **3**$^-$ and Imz, as shown in eq 5, is significantly reduced from 37.9 kcal mol^{-1} in a homogeneous dielectric medium (ε = 4.0) to 9.8 kcal mol^{-1} in the present model.

$$3(O_XH, N_1H, O_YH)^0 + Imz \rightarrow 3^-(O_X, N_1H, O_YH)^- + ImzH^+ \quad (5)$$

Our suggestion is that, apart form a significant salt-bridge interaction between **3**$^-$ and ImzH$^+$, relatively small modulation by the cation$-\pi$ interaction between ImzH$^+$ and the aromatic ring of Ind[29] is important for the regulation of pK_a.[58] Experimental support for this suggestion might be provided by a series of site-directed mutagenesis studies that replace six tryptophan residues in aequorin by a phenylalanine residue. One of the mutants, W86F, gave a bimodal emission spectrum at 455 and 400 nm with various bioluminescence activities (9.2−45.6%).[14f] The new band with λ_{max} = 400 nm in the W86F mutant was assigned to the neutral form of **4** (O_XH, N_1H, O_YH)^0.[14f] Such a spectral shift was also observed for the mutants of obelin, W92F, W92H, W92K, W92E, and W92R (Trp92 in obelin corresponds to Trp86 in aequorin).[60] Mutation of His16 is also expected to provide important information, since it is assumed to be a base in our model. Mutant aequorin with His16 replaced with Phe, which cannot serve as a proton acceptor, almost lost its function (0.1%),[14d] in agreement with our proposal. The replacement of His16 by Ala, however, still retained a luminescence activity, although less efficient (25.7%) than the wild type.[14d] The latter experimental fact apparently conflicts with our proposal that the presence of a base is essential for the preferential generation of a singlet state, which suggests a modification of our model. This led us to formulate an alternative mechanism that multiple protonation states could be responsible for the bioluminescence activity but with different efficiencies. As possible candidates for such a second protonation state in the H16A mutant, we are left with the neutral state (O_XH, N_1H, O_YH)^0 and the two monoanion states (O_XH, N_1, O_YH)$^-$ and (O_XH, N_1H, O_Y)$^-$. As for the neutral state (O_XH, N_1H, O_YH)^0, environmental effects that polarize the electron distribution of the substrate in one direction are needed, since this protonation state tends to give a homolytic diradical TS (Figures 3A and 9B). Since the TS would lie close in energy for the homolysis versus CT-induced decomposition, as the dioxetanone functionality becomes a much better electron acceptor (or the substituent is modified into a much better electron donor), the CT diradical TS will be selectively more stabilized, thereby preferring the singlet over the triplet primary products. This can be achieved by the introduction of specific short-range electrostatic interactions. In this respect, we wish to emphasize the roles of a charged histidine in the Tyr184-His169-Trp173 triad motif as biological catalysis that activates the peroxide bond and operates the CT-induced luminescence in either a concerted or stepwise manner. This suggestion can be verified by a preliminary investigation using an extended model complex that contains **3**$^{\varepsilon}$ and 11 model molecules of amino acid residues and three crystal water molecules (1851 basis functions), as demonstrated in Figure 12. The presence of an imidazolium cation, a model of protonated H169, near the dioxetanone functionality is found to cause a strong charge polarization without a polarizing medium, even when the substrate is in the neutral state (O_XH, N_1H, O_YH)^0; compare Figure 12 with Figure 6 for two different ways of charge polarization. The present model system is, of course, not a faithful model to the actual protein environment, since some atoms with an asterisk are fixed to the X-ray coordinates during geometry optimizations (Figure 12); however, qualitative features would at least be effective, as far as the imidazolium cation, which, unlike Tyr184, is in an α-helix, is still present in the vicinity of a dissociating peroxide. Finally, we should not overlook the fact that the imidazolium cation can also create a downhill slop leading to the formation of a radical pair, **4**$^{\bullet}$ (O_X, N_1H, O_YH)$\cdots CO_2^{\bullet-}$, in the thermolysis of the phenoxide anion species **3**$^-$ (O_X, N_1H, O_YH)$^-$, at the CAM-B3LYP/6-31G(d) level,[61] as shown in Figure 13. At the optimized local minimum, the C_2-C_3 bond distance is calculated to be 3.3 Å, a spatially separated $CO_2^{\bullet-}$ molecule is positioned near the pyrazine ring at a distance of 2.8 Å, and singly occupied natural orbitals ($n \approx 1.0$) are essentially localized on the $CO_2^{\bullet-}$ fragment and the oxidophenyl group. Such an appreciable "dip" never appears in a homogeneous dielectric medium without including explicit model molecules of amino acid residues, especially His169, Tyr184, and Trp173.

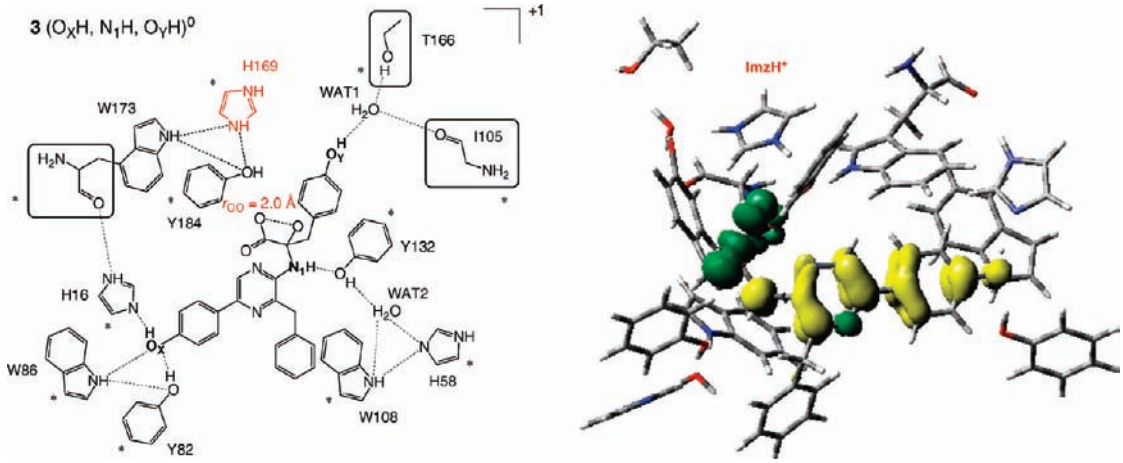

Figure 12. Spin density distribution of dissociating dioxetanone **3** $(O_XH, N_1H, O_YH)^0$ in the extended model, at the B3LYP/6-31G(d) level. The total charge of the system is +1. Atoms marked with an asterisk are kept frozen in geometry optimizations. Up and down spins are green and yellow. The reason why we set the total charge to be +1, rather than neutral, is that the imidazolium cation (protonated His169) has a cation-π interaction with the aromatic ring of the side group at the C_2 position of **3**.

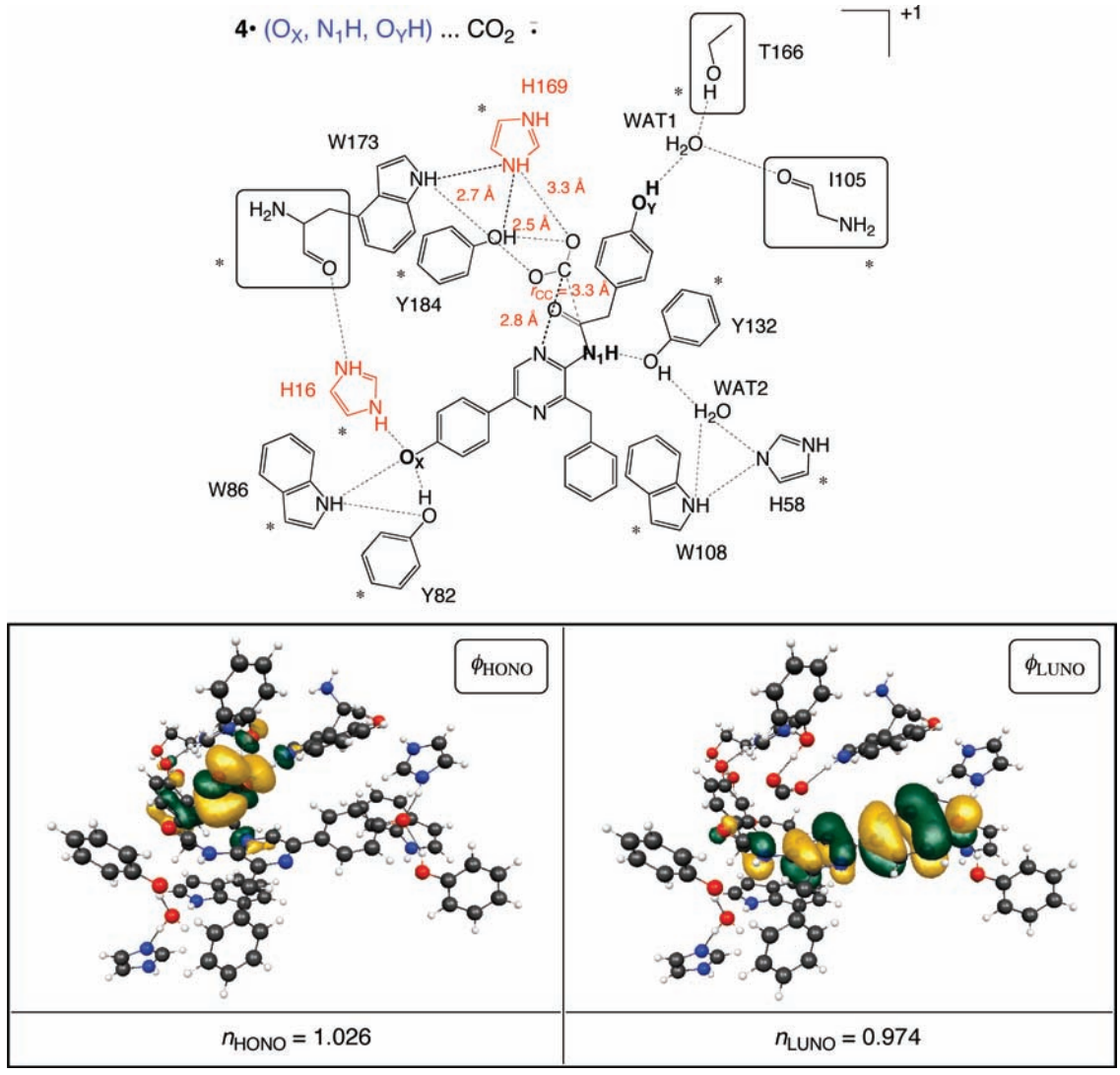

Figure 13. Geometrical parameters, highest occupied (ϕ_{HONO}) and lowest unoccupied (ϕ_{LUNO}) natural orbitals, and their occupation numbers (n_{HONO} and n_{LUNO}) for the local minimum of radical pair **4**•$(O_X, N_1H, O_YH)\cdots CO_2^{\bullet-}$ in the extended model, at the CAM-B3LYP/6-31G(d) level. The total charge of the system is +1. Atoms marked with an asterisk are kept frozen in geometry optimizations.

4. Conclusions

Theoretical investigation of thermal decomposition of peroxidized coelenterazines **3**^{z} under various conditions have revealed that external perturbations cause a significant change in the electronic property and stability of the peroxide, which may be critical for the bioluminescence activity. The balance

of homolytic and CT diradical contributions of the dissociating peroxide varies depending on the protonation state of the substrate and the polarity and hydrogen-bonding capability of the protein environment.

In the neutral state, $(O_XH, N_1H, O_YH)^0$, a polarizing medium is important, since it can generate an intramolecular CT diradical species with a large dipole moment that is better solvated by its reaction field; otherwise, the peroxide decomposes by a homolytic O−O dissociation with a high activation barrier (16.4 kcal mol^{-1}). In the amido anion state, $(O_XH, N_1, O_YH)^-$, two TSs, which are quite distinct from each other in terms of geometry, energetics, and electronic property, are available in the decomposition of the peroxide. The reaction will occur via a lower-lying CT diradical TS with a barrier of 9.3 kcal mol^{-1} rather than the higher-lying homolytic diradical TS, which is insensitive to a solvent polarity. The phenoxide anion group is found to be a sufficiently good electron donor to activate the O−O bond with a minimum barrier of 1.5 kcal mol^{-1}.

The present study deduces two mechanisms by which the neutral species can be activated under the catalysis by protein environment. The first mechanism is to enhance the ability of a substituent of the substrate to donate an electron. This can be accomplished by the conversion of the protonation state into the phenoxide anion, $(O_X, N_1H, O_YH)^-$ [or other anionic species (not investigated in this study)], which activate the substrate and thereby enables it to undergo the CT-induced decomposition without a polarizing medium. This finding highlights the importance of the pK_a regulation of the peroxide by environment. The analysis using simple model clusters suggests that a subtle stacking effect of the Tyr82-His16-Trp86 triad motif reduces the proton affinity of the oxido (O_X) anion moiety through horizontal hydrogen bonds and a vertical cation−π interaction. The second mechanism that can be reached from this study is to develop the electron-accepting capability of the O−O bond itself by another triad motif, Tyr184-His169-Trp173. In this respect, the regiochemical control in the oxygenation reaction of coelenterazine by O_2 for the formation of the dioxetanone functionality, rather than the dioxetane functionality, is shown to be important for the preferential generation of primary products in a singlet state. His169 in the triad can receive one proton that is relayed from the coelenterazine−2-hydroperoxide adduct via Tyr184. The resulting imidazolium cation acts to stabilize selectively the pathway for the CT-induced decomposition via a specific electrostatic interaction without a polarizing medium, even if the substrate is in the neutral state. The combination of the above two mechanisms brings about an intriguing result: the presence of both the imidazolium cation and phenoxide anion group causes a strong thermodynamic driving force for complete electron transfer, and consequently, create a downhill slope leading to the formation of a radical pair trapped momentarily in the nearby triad motif, which is made explicit in an appreciable "dip" on the potential surface. This event could affect the bioluminescence efficiency through either a decay or excitation process under a large fluctuation of the protein.

The first and second mechanisms can be understood in a more general sense that the behaviors of labile electrons can be controlled by the proton activity of a surrounding reaction field via a hydrogen-bond interface. The proton transfer occurs in an intermolecular manner from the substrate to one of the three Tyr-His-Trp triad motifs, which triggers a coupled electron transfer in an intramolecular manner from one of the potent electron-donating moieties to the dissociating peroxide bond. Thus, the Tyr-His-Trp triad motifs act as catalysts that activate the peroxide bond via proton relay and makes the pathway for CT-induced luminescence preferred within the photoprotein. Such a phenomenon is often observed in a wide range of biochemical processes and can be encompassed by a class of proton-coupled electron transfer.[62] Our study indicates that it might become possible to gain fundamental insight into the roles of key amino acid residues and to make contributions toward our understanding of the detailed mechanistic aspects of how the excitation on the chromophore occurs in aequorin. Resolution of the problems is the challenge for future studies.

Acknowledgment. H.I. is grateful to Prof. S. Kuramitsu for financial assistance of this research through the National Project on Protein Structural and Functional Analyses from the Ministry of Education, Culture, Sports, Science and Technology (MEXT), Japan. This study is supported in part by the New Energy and Industrial Technology Development Organization (NEDO).

Supporting Information Available: Complete ref 18; 8 figures of energy profiles, spin density distributions, geometrical parameters, HONOs and LUNOs, and intermolecular interactions; 7 tables of energies, bond lengths, diradical characters, decomposition mechanism classifications; and Cartesian coordinates and absolute energies of optimized structures reported. This material is available free of charge via the Internet at http://pubs.acs.org.

References and Notes

(1) (a) Shimomura, O.; Johnson, F. H.; Saiga, Y. *J. Cell. Comp. Physiol.* **1962**, *59*, 223. (b) Shimomura, O.; Johnson, F. H.; Saiga, Y. *Science* **1963**, *140*, 1339. (c) Johnson, F. H.; Shimomura, O. *Methods Enzymol.* **1978**, *57*, 271. (d) Ohmiya, Y.; Hirano, T. *Chem. Biol.* **1996**, *3*, 337.

(2) Cambell, A. K. *Biochem. J.* **1974**, *143*, 411.

(3) Herring, P. J. *Mar. Biol.* **1979**, *53*, 223.

(4) Shimomura, O.; Johnson, F. H.; Saiga, Y. *J. Cell. Comp. Physiol.* **1963**, *62*, 9.

(5) Levine, L. D.; Ward, W. W. *Comp. Biochem. Physiol.* **1982**, *72B*, 77.

(6) (a) Ward, W. W.; Seliger, H. H. *Biochemistry* **1974**, *13*, 1491. (b) Ward, W. W.; Seliger, H. H. *Biochemistry* **1974**, *13*, 1500.

(7) (a) Nakajima-Shimada, J.; Iida, H.; Tsuji, F. I.; Anraku, Y. *Proc. Natl. Acad. Sci. U.S.A.* **1991**, *88*, 6878. (b) Rizzuto, R.; Simpson, A. W. M.; Brini, M.; Pozzan, T. *Nature* **1992**, *358*, 325.

(8) (a) Inouye, S.; Noguchi, M.; Sakaki, Y.; Takagi, Y.; Miyata, T.; Iwanaga, S.; Miyata, T.; Tsuji, F. I. *Proc. Natl. Acad. Sci. U.S.A.* **1985**, *82*, 3154. (b) Charbonneau, H.; Walsh, K. A.; McCann, R. O.; Prendergast, F. G.; Cormier, M. J; Vanaman, T. C. *Biochemistry* **1985**, *24*, 6762.

(9) Head, J. F; Inouye, S.; Teranishi, K.; Shimomura, O. *Nature* **2000**, *405*, 372.

(10) (a) Shimomura, O. *Biophys. Res. Commun.* **1995**, *211*, 359. (b) Shimomura, O.; Inouye, S. *Biophys. Res. Commun.* **1996**, *221*, 77.

(11) Shimomura, O.; Johnson, F. H. *Proc. Natl. Acad. Sci. U.S.A.* **1978**, *75*, 2611.

(12) (a) Shimomura, O.; Johnson, F. H. *Biochem. Biophys. Res. Commun.* **1971**, *44*, 340. (b) Teranishi, K.; Ueda, K.; Nakano, M.; Hisamatsu, M.; Yamada, T. *Tetrahedron Lett.* **1994**, *35*, 8181. (c) Usami, K.; Isobe, M. *Tetrahedron Lett.* **1995**, *36*, 8613. (d) Mori, K.; Maki, S.; Niwa, H.; Ikeda, H.; Hirano, T. *Tetrahedron* **2006**, *62*, 6272. (e) Teranishi, K. *Bioorg. Chem.* **2007**, *35*, 82.

(13) Teranishi, K; Goto, T. *Bull. Chem. Soc. Jpn.* **1990**, *63*, 3132.

(14) (a) Kurose, K.; Inouye, S.; Sasaki, Y.; Tsuji, F. I. *FEBS Lett.* **1989**, *86*, 80. (b) Nomura, M.; Inouye, S.; Ohmiya, Y; Tsuji, F. I. *FEBS Lett.* **1991**, *295*, 63. (c) Watkins, N. J.; Campbell, A. K *Biochem. J.* **1993**, *293*, 181. (d) Ohmiya, Y.; Tsuji, F. I. *FEBS Lett.* **1993**, *320*, 267. (e) Tsuji, F. I.; Inouye, S.; Goto, T.; Sasaki, Y. *Proc. Natl. Acad. Sci. U.S.A.* **1986**, *83*, 8107. (f) Ohmiya, Y.; Ohashi, M.; Tsuji, F. I. *FEBS Lett.* **1992**, *301*, 197.

(15) (a) Shimomura, O.; Musicki, B.; Kishi, Y. *Biochem. J.* **1988**, *251*, 405. (b) Shimomura, O.; Musicki, B.; Kishi, Y. *Biochem. J.* **1989**, *261*, 913. (c) Shimomura, O.; Inouye, S.; Musicki, B.; Kishi, Y. *Biochem. J.* **1990**, *270*, 309. (aa) Shimomura, O.; Kishi, Y.; Inouye, S. *Biochem. J.* **1993**, *296*, 549.

(16) Hirano, T.; Negishi, R.; Yamaguchi, M.; Chen, F. Q.; Ohmiya, Y.; Tsuji, F. I.; Ohashi, M. *J. Chem. Soc., Chem. Commun* **1995**, 1335.

(17) (a) Hori, K.; Wampler, J. E.; Cormier, M. J. *Chem. Commun.* **1973**, 492. (b) Shimomura, O.; Teranishi, K. *Luminescence* **2000**, *15*, 51. (c) Imai, Y.; Shibata, T.; Maki, S.; Niwa, H.; Ohashi, M.; Hirano, T. *J. Photochem. Phtobiol. A* **2001**, *146*, 95.

(18) Frisch, M. J.; et al. *Gaussian 03*, revision E.01; Gaussian, Inc.: Wallingford, CT, 2004.

(19) (a) Becke, A. D. *Phys. Rev. A* **1988**, *38*, 3098. (b) Lee, C.; Yang, W.; Parr, R. G. *Phys. Rev. B* **1988**, *37*, 785. (c) Becke, A. D. *J. Chem. Phys.* **1993**, *98*, 5648.

(20) Hehre, W. J.; Radom, L.; Schleyer, P. v. R.; Pople, J. A. *Ab Initio Molecular Orbital Theory*; Wiley: New York, 1986.

(21) (a) Klamt, A.; Schüürmann, G. *J. Chem. Soc., Perkin Trans. 2* **1993**, 799. (b) Andzelm, J.; Kölmel, C.; Klamt, A. *J. Chem. Phys.* **1995**, *103*, 9312. (c) Barone, V.; Cossi, M. *J. Phys. Chem. A* **1998**, *102*, 1995. (d) Cossi, M.; Rega, N.; Scalmani, G.; Barone, V. *J. Comput. Chem.* **2003**, *24*, 669.

(22) Gilson, M. K.; Honig, B. H. *Biopolymers* **1986**, *25*, 2097.

(23) Yanai, T.; Tew, D. P.; Handy, N. C. *Chem. Phys. Lett.* **2004**, *393*, 51.

(24) (a) Dreuw, A.; Weisman, J. L.; Head-Gordon, M. *J. Chem. Phys.* **2003**, *119*, 2943. (b) Kobayashi, R.; Amos, R. D. *Chem. Phys. Lett.* **2006**, *420*, 106.

(25) Schmidt, M. W.; Baldridge, K. K.; Boatz, J. A.; Elbert, S. T.; Gordon, M. S.; Jensen, J. J.; Koseki, S.; Matsunaga, N.; Nguyen, K. A.; Su, S.; Windus, T. L.; Dupuis, M.; Montgomery, J. A. *J. Comput. Chem.* **1993**, *14*, 1347.

(26) Löwdin, P.-O. *Phys. Rev.* **1955**, *97*, 1474.

(27) Yamaguchi, K. In *Self-Consistent Field: Theory and Applications*; Carbo, R., Klobukowski, M., Eds.; Elsevier: Amsterdam, 1990; p 727. (b) Isobe, H.; Takano, Y.; Kitagawa, Y.; Kawakami, T.; Yamanaka, S.; Yamaguchi, K.; Houk, K. N. *Mol. Phys.* **2002**, *100*, 717. (c) Isobe, H.; Takano, Y; Kitagawa, Y.; Kawakami, T.; Yamanaka, S.; Yamaguchi, K.; Houk, K. N. *J. Phys. Chem. A* **2003**, *107*, 682.

(28) Isobe, H.; Yamanaka, S.; Kuramitsu, S.; Yamaguchi, K. *J. Am. Chem. Soc.* **2008**, *130*, 132.

(29) (a) Dougherty, D. A. *Science* **1996**, *271*, 163. (b) Ma, J. C.; Dougherty, D. A. *Chem. Rev.* **1997**, *97*, 1303. (c) Meyer, E. A.; Castellano, R. K.; Diedereich, F. *Angew. Chem., Int. Ed.* **2003**, *42*, 1210.

(30) Rough estimates using the X-ray coordinates containing $\mathbf{2}^{z}$ (204 atoms, non-optimized) indicates that, in the cationic environment, the energies of the protonation states of $\mathbf{2}^{z}$, (O_XH, N_1, O_YH), (O_X, N_1H, O_YH), and (O_X, N_1, O_YH)$^-$, which correspond to (O_XH, N_1, O_YH)$^-$, (O_X, N_1H, O_YH)$^-$, and (O_X, N_1, O_YH)$^{2-}$ of $\mathbf{3}^{z}$, relative to (O_XH, N_1H, O_YH)$^+$, are 12.7, 2.8, and 21.1 kcal mol^{-1}, at the B3LYP/6-31G(d) level. The neutral environment, however, stabilizes (O_X, N_1, O_YH)$^-$, while destabilizing (O_XH, N_1, O_YH) and (O_X, N_1H, O_YH), to such an extent that (O_X, N_1H, O_YH) and (O_X, N_1, O_YH)$^-$ lie 50.9 and 6.1 kcal mol^{-1} above (O_XH, N_1, O_YH). Of course, these values have to be revised in a more sophisticated manner.

(31) Actually, the $C_2-N_1-C_9$ bond angle is 118.4° at the equilibrium geometry of $\mathbf{3}^-$ (O_XH, N_1, O_YH)$^-$, 107.4° at the homolytic diradical TS, and 119.3° at the CT diradical TS.

(32) The orbital splitting is roughly 0.011 au at the equilibrium geometry of $\mathbf{3}^-$ (O_XH, N_1, O_YH)$^-$; rehybridization will further affect orbital energies during the reaction.

(33) Actually, 2-peroxide anion does not have a local minimum in the gauche conformation. The relative energy of 2-peroxide structure in Figure 4 is roughly estimated by assuming the geometry of 2-hydroperoxide intermediate with the gauche conformation, which is closely related with the one found at the X-ray structure.[9]

(34) White, E. H.; Roswell, D. F.; Dupont, A. C.; Wilson, A. A. *J. Am. Chem. Soc.* **1987**, *109*, 5189.

(35) For comparison, the results for the higher-lying TS of the amido anion state (O_XH, N_1, O_YH)$^-$ are presented in Figure S2, Supporting Information. Contrary to the neutral case, a polarizing medium has little effect on the spin density distribution of the dissociating peroxide.

(36) Hirano, T.; Takahashi, Y.; Kondo, H.; Maki, S.; Kojima, S.; Ikeda, H.; Niwa, H. *Photochem. Photobiol. Sci.* **2008**, *7*, 197.

(37) (a) Catalani, L. H.; Wilson, T. *J. Am. Chem. Soc.* **1989**, *111*, 2633. (b) McCapra, F. *J. Photochem. Photobiol. A* **1990**, *51*, 21.

(38) (a) Schuster, G. B. *Acc. Chem. Res.* **1979**, *12*, 366. (b) McCapra, *J. Chem. Soc., Chem. Commun.* **1977**, 946.

(39) (a) Adam, W.; Bronstein, I.; Trofimov, A. V.; Vasil'ev, R. F. *J. Am. Chem. Soc.* **1999**, *121*, 958. (b) Adam, W.; Trofimov, A. V. *J. Org. Chem.* **2000**, *65*, 6474. (c) Adam, W.; Matsumoto, M.; Trofimov, A. V. *J. Am. Chem. Soc.* **2000**, *122*, 8631.

(40) Isobe, H.; Takano, Y.; Okumura, M.; Kuramitsu, S.; Yamaguchi, K. *J. Am. Chem. Soc.* **2005**, *127*, 8667.

(41) (a) Devadoss, C.; Bharathi, P.; Moore, J. S. *J. Am. Chem. Soc.* **1996**, *118*, 9635. (b) Shortreed, M. R.; Swallen, S. F.; Shi, Z.-Y.; Tan, W.; Xu, Z.; Devadoss, C.; Moore, J. S.; Kopelman, R. *J. Phys. Chem. B* **1997**, *101*, 6318. (c) Tretiak, S.; Chernyak, V.; Mukamel, S. *J. Phys. Chem. B* **1998**, *102*, 3310.

(42) Matsumoto, M.; Watanabe, N. *Bull. Chem. Soc. Jpn.* **2005**, *78*, 1899.

(43) Relative energies of primary products to $\mathbf{3}^{z}$ are summarized in Table S2, Supporting Information. The thermodynamic driving forces for electron-transfer reaction for (O_XH, N_1H, O_YH), (O_XH, N_1, O_YH)$^-$, (O_X, N_1H, O_YH)$^-$, and (O_X, N_1, O_YH)$^{2-}$ are calculated to be +60.7,−29.5,−40.6, and−113.4 kcal mol^{-1} in the gas phase, +11.5,−46.3,−51.9, and−97.6 kcal mol^{-1} in benzene, and−26.1,−58.3,−58.6, and−84.6 kcal mol^{-1} in acetonitrile. See also Figure 4 in ref 28.

(44) Vallee, B. L.; Williams, R. J. P. *Proc. Natl. Acad. Sci. U.S.A.* **1968**, *59*, 498.

(45) Chung, L. W.; Hayashi, S.; Lundberg, M.; Nakatsu, T.; Kato, H.; Morokuma, K. *J. Am. Chem. Soc.* **2008**, *130*, 12880.

(46) *Organometallic Conjugation: Structures, Reactions and Functions of d-d and d-π Conjugated Systems*; Nakamura, A., Ueyama, N., Yamaguchi, K., Eds.; Springer: Berlin, 2003; p 339.

(47) During the decomposition of $\mathbf{3}^{z}$, a protonated histidine is assumed to be present near the carbonyl oxygen of coelenterazine (at a distance of about 3.4 Å in the case of the X-ray crystal structure of aequorin; see Figure 1) through a proton delivery that allows the hydroperoxide form of coelenterazine $\mathbf{2}^{z}$ to undergo a ring closure leading to $\mathbf{3}^{z}$. Preliminary investigation has indicated that an imidazolium cation ($ImzH^+$) and a CO_2 radical anion can form a stable complex, $ImzH^+\cdots CO_2^{\bullet-}$ with the complexation energy of about−13 (−22) kcal mol^{-1} with (without) the entropic change upon complexation$-T\Delta S$, at the CPCM B3LYP/6-31+G(d) level ($\varepsilon = 4.0$); see Figure S3 (Supporting Information) for details. For the proton-relay mechanism, see: Vysotski, E. S.; Lee, J. *Acc. Chem. Res.* **2004**, *37*, 405.

(48) Marcus, R. A.; Sutin, N. *Biochim. Biophys. Acta* **1985**, *811*, 265.

(49) (a) Shimomura, O.; Johnson, F. H.; Morise, H. *Biochemistry* **1974**, *13*, 3278. (b) Shimomura, O.; Johnson, F. H. *Proc. Natl. Acad. Sci. U.S.A.* **1978**, *75*, 2611. (c) Teranishi, K.; Isobe, M.; Yamada, T.; Goto, T. *Tetrahedron Lett.* **1992**, *33*, 1303. (d) Teranishi, K.; Ueda, K.; Hisamitsu, M.; Yamada, T. *Biosci. Biotech. Biochem.* **1995**, *59*, 104.

(50) Isobe H.; Yamanaka, S.; Okumura, M.; Yamaguchi, K. In *Proceedings of the 15th International Symposium on Bioluminescence and Chemiluminescence: Light Emission: Biology and Scientific Applications*; Shen, X., Yang, X.-L., Zhang, X.-R., Cui, Z. J., Kricka, L. J., Stanley, P. E., Eds.; World Scientific: Singapore, 2008; p 119.

(51) We have also examined the effects of polarization functions on hydrogen atoms and diffuse functions on heavy atoms on the flexibility in the description of hydrogen bonds and the geometries and energetics of anionic species in the thermolysis of phenoxide-anion-substituted dioxetanes and dioxetanones, as suggested by a reviewer (Table S3, Supporting Information). All basis sets examined [6-31G(d), 6-31+G(d), and 6-31+G(d,p)] give virtually the same qualitative trends. Quantitative differences are within 2.9 kcal mol^{-1} in the activation barrier and 0.256 Å in the optimized O−O bond length at a TS. Compare also Table S1 (Supporting Information) [6-31G(d) results for $\mathbf{3}^{z}$] with Table 1 [6-31+G(d)].

(52) The proton affinities of $\mathbf{2}^{z}$, $\mathbf{3}^{z}$, $\mathbf{5}^+$, and **6** in organic solvents have been estimated theoretically (Tables S4, S5, S6, and S7, Supporting Information).

(53) Since the N_7 position of $\mathbf{6}^-$ is a good proton receptor (Table S7, Supporting Information), a model system that consists of $\mathbf{6H}^-$ (O_X, N_1, O_YH)$^-$ (the N_7 position is protonated) + $ImzH^+$ + PhOH + Ind has also been examined. The calculated potential curve and geometrical transformation for the O−O bond elongation of $\mathbf{6H}^-$ shows that dissociating $\mathbf{6H}^-$ behaves similarly to $\mathbf{6}^-$; i.e., a drastic electronic reorganization from homolytic diradical to CT diradical occurs during the reaction (Figure S4, Supporting Information).

(54) See Figure S5 (Supporting Information) for the shapes of HONO and LUNO at $r_{OO} = 1.9$ and 2.0 Å of $\mathbf{6}^-$.

(55) Actually, the $O-C_5-C_6-O$ four-membered ring of $\mathbf{6}^-$ is slightly twisted about the C_5-C_6 bond by 10.8° at $r_{OO} = 2.0$ Å. The same is true of $\mathbf{3}^-$, which have−7.2° twisted structure at $r_{OO} = 2.0$ Å.

(56) The converse holds for the neutral state, **1** (O_XH, N_1H, OH), for which the 2-hydroperoxide form, $\mathbf{2}^+$ (O_XH, N_1H, O_YH)$^+$, is more stabilized by ca. 6−7 kcal mol^{-1} than the corresponding 5-hydroperoxide, $\mathbf{5}^+$ (O_XH, N_1H, O_YH)$^+$.

(57) According to the Curtin−Hammett principle, even if there is some barrier for the proton transfer between the competing CT and homolytic diradical (HD) TSs, the ratio of the CT to HD trajectories is determined by $\Delta\Delta G^{\ddagger}_{CT\text{-}HD}$ as CT/HD = $\exp(-\Delta\Delta G^{\ddagger}_{CT\text{-}HD}/RT)$.

(58) Since the B3LYP method does not account for dispersion interaction, we re-evaluated the equilibrium geometries of the model complex by the two-layered ONIOM method[59] [MP2/6-31G(d):B3LYP/6-31G(d)]. Based on the ONIOM optimized geometries, the interaction energy between Ind and $ImzH^+$ (Imz) is calculated to be−17.6 (−7.7) kcal mol^{-1} at the MP2/6-31G(d) level (gas phase), among which the electrostatic energy is−12.6 (−5.7) kcal mol^{-1} at the HF/6-31G(d) level (Figure S7, Supporting Information).

(59) (a) Dapprich, S.; Komáromi, I.; Byun, K. S.; Morokuma, K.; Frisch, M. J. *J. Mol. Struct. (THEOCHEM)* **1999**, *461*−*462*, 1. (b) Maseras, F.; Morokuma, K. *J. Comput. Chem.* **1995**, *16*, 1170.

(60) (a) Vysotski, E. S.; Liu, Z.-J.; Markova, S. V.; Blinks, J. R.; Deng, L.; Frank, L. A.; Herko, M.; Malikova, N. P.; Rose, J. P.; Wang, B.-C; Lee, J. *Biochemistry* **2003**, *42*, 6013. (b) Markova, N. P.; Stepanyuk, G. A.; Frank, L. A.; Markova, S. V.; Vysotski, E. S.; Lee, J. *FEBS Lett.* **2003**, *554*, 184.

(61) Similarly to the CAM-B3LYP method, the BHandHLYP functional, which includes 50% of the Hartree−Fock exchange functional, could locate a radical pair on the potential surface (Figure S8, Supporting Information). On the other hand, B3LYP calculations either diverged or collapsed into the closed-shell ground state.

(62) Huynh, M. H. V.; Mayer, J. M. *Chem. Rev.* **2007**, *107*, 5004.

JP905401B